AD-A139 653 HIGH STRENGTH HERMETICALLY COATED OPTICAL FIBERS(U) 1/1
HEWLETT-PACKARD CO PALO ALTO CALIF SOLID STATE LAB
E G HANSON ET AL. 31 MAR 81 N00123-80-C-0245

UNCLASSIFIED F/G 20/6 NL

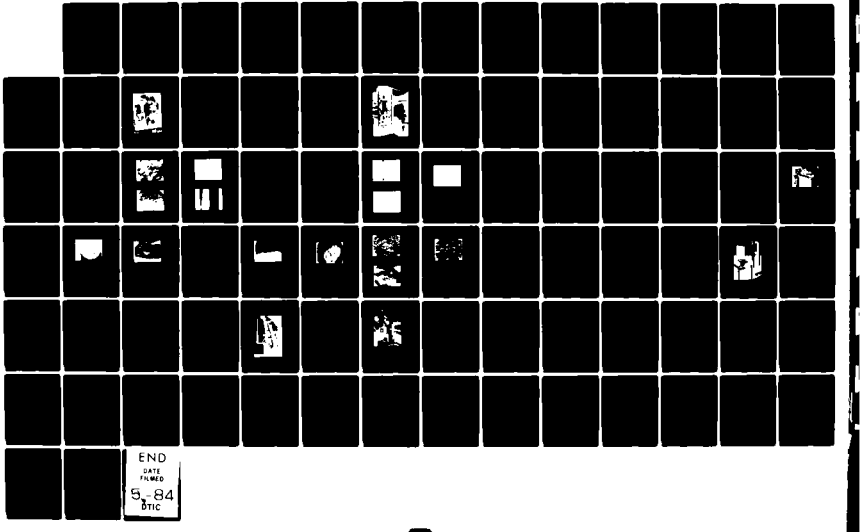

END
DATE FILMED
5-84
DTIC

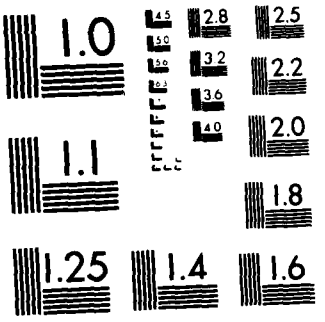

HEWLETT-PACKARD COMPANY
Solid State Laboratories
1501 Page Mill Road
Palo Alto, California 94304

HIGH STRENGTH HERMETICALLY COATED OPTICAL FIBERS

by

E. G. Hanson, C. A. Schantz and R. Hiskes

FINAL TECHNICAL REPORT

1 January 1980 - 31 March 1981

Contract No. N00123-80-C-0245

A Research Project Sponsored By the
Naval Ocean Systems Center
San Diego, California 92152

ABSTRACT

Static fatigue resistance of optical fibers has been achieved through passivation of the fiber surface by a novel CVD silicon oxynitride coating which is deposited on-line during fiber pulling. Static fatigue susceptibility less than one-sixth that of conventional fiber has been achieved. In addition, high proof stress yields have been achieved at 2.1 GPa (300,000 psi). In tests of the most recent 21,150 m of MCVD fiber proof tested at 2.1 GPa, nine pieces longer than 900 m passed the test.

ACKNOWLEDGEMENTS

We are pleased to acknowledge the able assistance of Caroline Scott and Marti Narbut for providing preforms, Laurie Stromsheim and André Nel for drawing the fiber and coating it with silicon oxynitride; of John Feustel and Jim Williamson in testing the mechanical and optical properties, of Marty Maez in SEM fracture surface analysis; and of Marianne Guerin-Brown, Paul Courtney, and Yale Strausser in Auger analysis. Bob Burmeister has provided advice and encouragement important to all phases of the project.

Table of Contents

		Page
1.0	Introduction	1
2.0	Fiber Fabrication	5
	2.1 Specifications	5
	2.2 Preform Fabrication	6
	2.3 Fiber Drawing	10
	2.4 Silicon Oxynitride Deposition	14
3.0	Silicon Oxynitride Characterization	17
	3.1 Auger Analysis	18
	3.2 Surface Morphology	21
	3.3 Etching Studies	25
4.0	Fiber Strength	28
	4.1 Intrinsic Strength of Optical Fibers	28
	4.2 Weak Flaws	32
	4.3 Experimental Results	45
	4.3.1 Instron Tensile Test	45
	4.3.2 20 Meter Tensile Test	50
	4.3.3 Proof Test	53
	4.3.4 Bend Fracture Test	57
	4.3.5 Temperature Effects	59
	4.3.6 Aging Effects	61
5.0	Fiber Fatigue	63
	5.1 Introduction	63
	5.2 Dynamic Fatigue Results	66
	5.3 Static Fatigue Results	66
	5.4 Cyclic Fatigue	63
6.0	Optical Properties	74
7.0	Conclusions	76
8.0	References	77

LIST OF FIGURES

FIGURE NO.		PAGE
1.	Schematic of crack growth in optical fiber subjected to static stress leading to eventual static fatigue failure.	2
2.	MCVD preform fabrication.	7
3.	MCVD lathe showing pyrometer and TV camera for automated temperature and diameter control.	8
4.	Schematic of the fiber puller.	11
5.	Optical fiber drawing tower and associated elecronics.	12
6.	Data logged during a fiber draw.	13
7.	Silicon oxynitride CVD reactor.	15
8.	Auger depth profile of silicon oxynitride coated fiber.	19
9.	SEM photo of silicon oxynitride deposited on an optical fiber at 1000°C temperature (10,000 X)	22
10.	SEM photo of silicon oxynitride deposited on an optical fiber at 1100°C (10,000 X).	22
11.	SEM photo of silicon oxynitride deposited on an optical fiber at 800°C (10,000 X).	23
12.	SEM photo of featureless silicon oxynitride film deposited on an optical fiber at 1100°C (1,000 X).	23
13.	SEM photo of oxynitrided fiber (10,000 X).	26
14.	SEM photo of oxynitrided fiber after 10 s in HF (10,000 X).	26
15.	SEM photo of oxynitrided fiber after 20 s in HF (10,000 X).	27
16.	SEM photo of a fracture surface originating from a 0.35 GPa flaw.	33
17.	SEM photo of scratch at origin of .35 GPa prooftest break (500 X).	35
18.	SEM photo of a weak flaw caused by porosity in the fiber which generated a 2.1 GPa prooftest break (20,000 X).	36

(LIST OF FIGURES CONT.)

FIGURE NO.		PAGE
19.	SEM photo of an inclusion just inside the edge of the fiber which caused a 1.4 GPa prooftest break (2000 X).	38
20.	SEM photo of shattered surface of fiber fractured at a stress of 1.4 GPa.	39
21.	As-received ZrO_2 furnace tube (1000 X).	40
22.	ZrO_2 furnace tube after washing (5000 X).	40
23.	ZrO_2 furnace tube after one thousand hours at 2000°C (200 X).	41
24.	Instron Model 1122 tensile tester.	46
25.	Typical data from Instron test of silicon oxynitride coated fiber.	48
26.	20 meter gauge length horizontal tensile tester.	52
27.	Proof tester for continuous tensile testing up to 45 N.	54
28.	Weibull plot of the strength distribution in a non-oxynitride coated fiber tested first at 9 sequentially higher proof test levels and then tested in the horizontal tensile tester.	56
29.	Bend test apparatus.	58
30.	Strength measured in bend test as a function of temperature for fiber 1252 (oxynitrided) compared to conventional (non-oxynitrided) fiber.	60
31.	Strength measured in bend test after varying durations of zero-stress aging in 22°C deionized water.	62
32.	Mean time to failure vs. static applied stress for typical conventional fiber with SiO_2 surface. Fast fracture strength = 4.9 GPa, u = 0.050 (n = 20).	65
33.	Static fatigue comparison between oxynitride coated fiber and conventional fiber at 22°C in air at 50% R.H.	69
34.	Static fatigue at 22°C for fibers immersed in deionized water, compared to Bell Labs data at 33°C and 90° R.H.	71
35.	Static fatigue data in 80°C water.	72
36.	Spectral attenuation of silicon oxynitride coated fiber.	75

LIST OF TABLES

TABLE NO.		PAGE
1.	Fiber specifications	5
2.	Yield of silicon oxynitride coated fibers prooftested at 2.1 GPa (304 kpsi).	44
3.	Tensile strength of 140 μm diameter silicon oxynitride coated HP fibers.	57
4.	Dynamic fatigue of 140 μm diameter silicon oxynitride coated HP fibers.	67

1.0 INTRODUCTION

High strength (0.7-2.1 GPa) fatigue resistant optical fibers are desirable for a variety of systems applications in lengths ranging from as little as 1 meter to 10-30 km or more. Optical fibers belong to that class of brittle ceramic materials which are susceptible to static fatigue or stress corrosion cracking.[1] Static fatigue is the stress assisted slow growth of microcracks leading eventually to catastrophic mechanical failure. It occurs via attack by atmospheric moisture and other ambient impurities as shown schematically in Fig. 1. There are a number of ways to guard against fiber fatigue including

(1) ensuring a low stress level by surrounding the fiber with strong (and expensive) cable,

(2) fabricating a very high strength fiber to ensure only small microcracks that won't grow to catastrophic size during the fiber lifetime (1-30 years),

(3) building in a surface compressive stress which must be overcome before microcracks will grow, and

(4) sealing the fiber (and existing crack) surface from the environment with a hermetic seal such as silicon oxynitride so that the cracks cannot grow.

Options(1) and (2) are quite expensive, and in fact (1) is an unacceptable choice for the military need of a lightweight, compact pay-out reel. Short gauge length (1-50 m) fibers can be made exceedingly strong, approaching 7 GPa, but it is generally accepted practice in the industry that for a non-fatigue resistant optical fiber, the proof stress level should be at least three times the service stress, and this results in unacceptably low production yields (approaching 0) for 2.1 GPa fiber

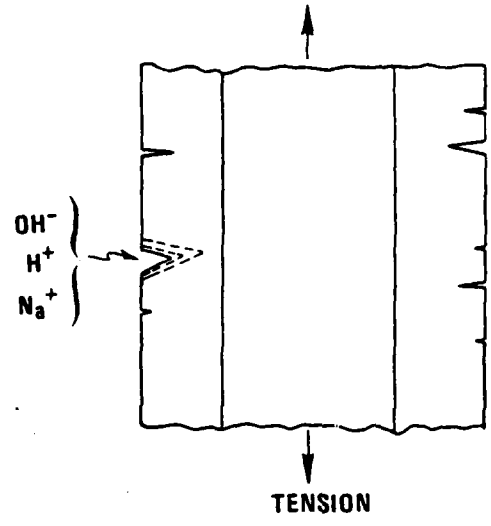

Figure 1. Schematic of crack growth in optical fiber subjected to static stress leading to eventual static fatigue failure.

in 1-10 km lengths. Compressive strengthening is an option which has produced strong fibers with a measurable increase in fatigue resistance,[2] but the most attractive alternative still remains a hermetic coating to protect the fiber against crack growth.

A number of different coatings have been applied to protect the surface including a variety of organic compounds,[3] metals[4] and carbon.[5] In this final report for Contract No. N00123-80-C-0245 we will focus on the strength and fatigue properties obtained at Hewlett-Packard by on line application of a thin, vitreous silicon oxynitride coating to the optical fiber.

The scope of this phase of the research effort includes:

(1) fabrication of silica clad preforms capable of yielding continuous lengths of fiber > 10 km long,

(2) drawing the preform to a fiber diameter either 125 μm or 140 μm in diameter,

(3) application of a pinhole free silicon oxynitride film which increases fiber resistance to static fatigue without introducing either weak flaws (< 2.1 GPa) or optical loss, and

(4) demonstration of fiber strength, fatigue resistance and microbending properties by extensive mechanical and optical characterization.

The principle results to date include generation of (1) large preforms containing 10 - 15 km of optical fiber, and (2) reproducible silicon oxynitride coated fibers with extremely tight and unimodal Weibull distributions which pass a 2.1 GPa prooftest in lengths exceeding 1 km, exhibit static fatigue parameters $u = 1/n^* < 0.01$ and have mean strengths of 2.8 GPa. These results are obtained by an atmospheric pressure chemical vapor deposition process at fiber draw rates of 0.3 - 1.2 m/s. Because of the high degree of fatigue resistance exhibited by these fibers, the proof stress required to assure a given static fatigue life is greatly reduced compared to that required for a conventional fiber. For example, to assure a lifetime of 30 years under 2.0 GPa static stress, the silicon oxynitride coated fiber would need to pass a 1 second proof stress at 2.35 GPa, while a conventional fiber would need to pass a 1 second proof stress at 5.40 GPa.

---

* n is the standard fracture mechanics coefficient which describes static fatigue. See for example, Reference 1.

2.0 FIBER FABRICATION

2.1 Specifications

In this program we have developed the silicon oxynitride coating process using both firepolished Suprasil$^{(TM)}$ rods and silica clad preforms made by the modified chemical vapor deposition (MCVD) process. The specifications for the optical properties of the MCVD fibers have been driven by military and data link specifications for such fibers as given in Table I.

TABLE I.

Fiber Specifications

Property	Data Link (Hewlett-Packard)	Military (NOSC Strong Fiber Program)
Core Diameter	100 μm	≥ 30 μm
Fiber Diameter	140 μm	125 μm (140 μm acceptable)
Attenuation	Cabled < 10 db/km @ 820 nm	Uncabled < 6 db/km @ 850 nm
Numerical Aperture	0.30	≥ 0.20 (nominal)
Bandwidth	20-200 MHz-km	≥ 20 MHz-km
Length	1 km	10-30 km
Strength	0.7 GPa prooftest	2.1 GPa prooftest
Fatigue Resistance	maximum	maximum

In general we have endeavored to meet the most stringent of the two sets of specifications as will be described in detail in the remainder of this section, which encompasses the MCVD preform process, the fiber drawing process and the silicon oxynitride coating process.

2.2 Preform Fabrication

The MCVD lathe is shown in Figs. 2 and 3. The MCVD process is fully automated, using an HP 9825 calculator with HP 6940 and HP 2240 processors to ensure run-to-run reproducibility. The lathe is housed in a laminar flow clean air hood to keep contaminants away from the surface of the preform.

The starting tube is a Heraeus-Amersil T08 WG SiO_2 tube 27 mm O.D. x 1 or 1.5 mm wall thickness. The 1 m long tube is joined at one end to a 5 cm diameter SiO_2 tube located at the exhaust end of the lathe which collects some of the excess soot deposited in the process. The tube is mounted on the lathe after a light rinse in HF followed by washing in TCE, and then firepolished at temperatures greater than 2000°C to clean both the inner and outer surfaces of the tube. An internal pressure control scheme maintains a constant tube diameter during both the firepolish and deposition stages. Despite extensive firepolishing, numerous light scattering centers sometimes remain on the tube surface, but most of these gradually disappear as the deposition proceeds.

In the standard process, a cladding layer of P_2O_5-SiO_2 or B_2O_3-SiO_2, is deposited in 10 torch passes, followed by a P_2O_5-GeO_2-SiO_2 core deposition of 65 passes. The tube is then collapsed to produce a finished

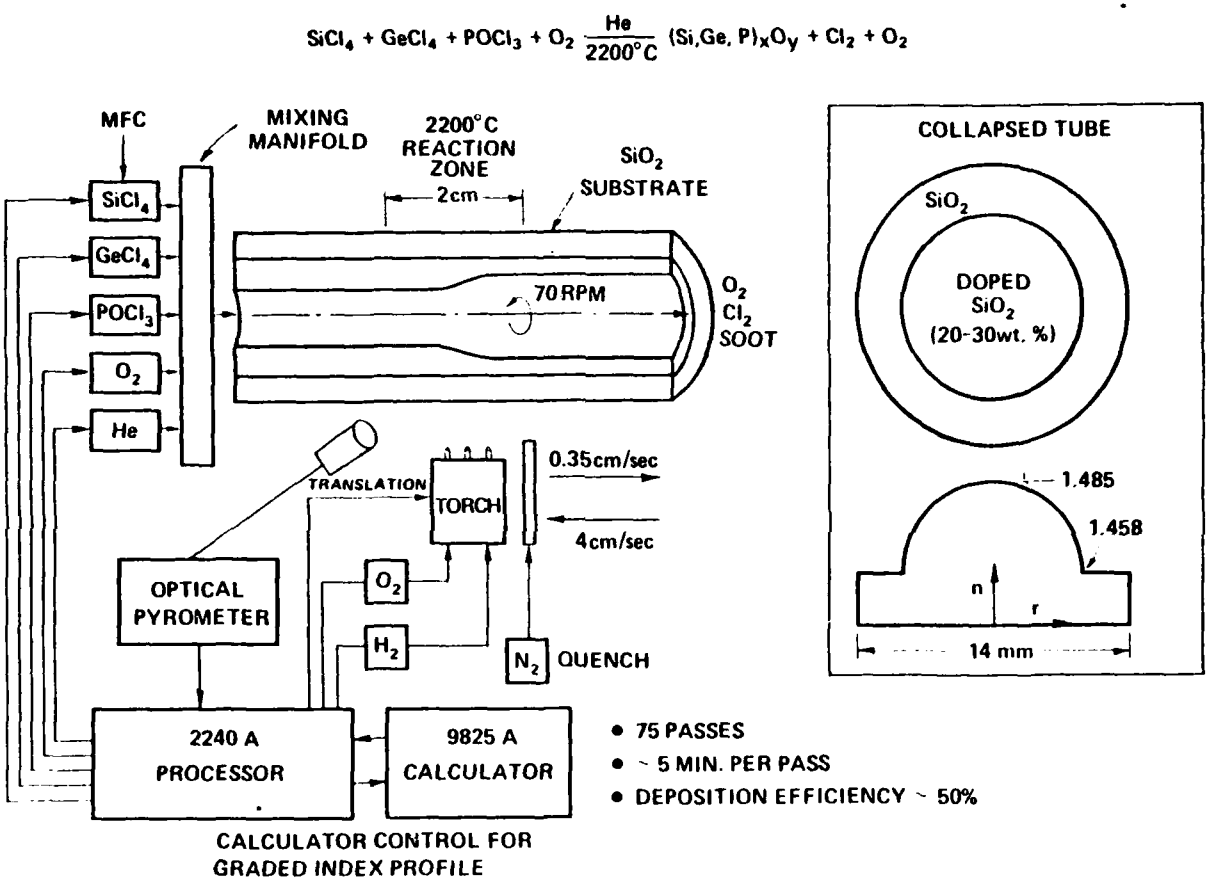

Figure 2. MCVD Preform Fabrication.

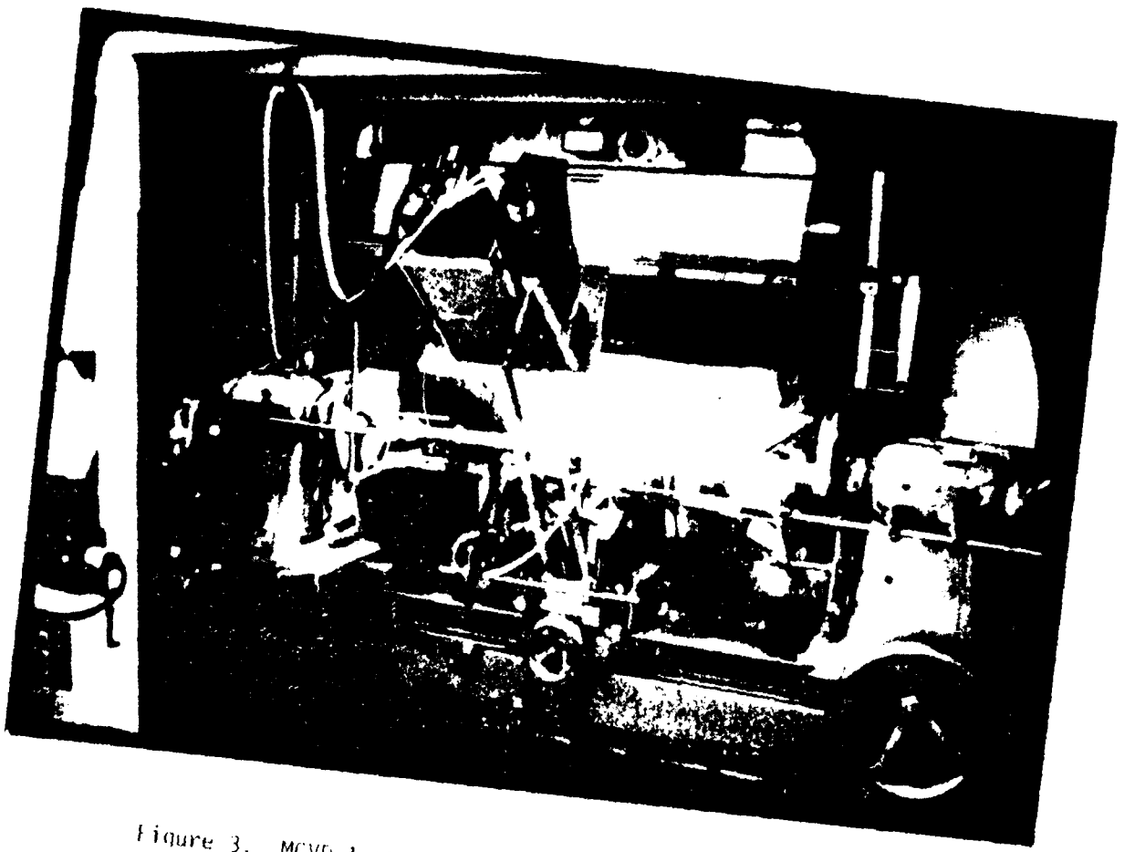

Figure 3. MCVD lathe showing pyrometer and TV camera for automated temperature and diameter control.

preform with outer diameter up to 17.5 mm. The steady state deposition length is 70 cm which yields > 10 km of 140 μm diameter fiber. During the collapsing process, the surface temperature of the preform exceeds 2300°C, and a significant amount of SiO_2 is vaporized from the surface, which prepares the preform for drawing into fiber without further cleaning. The average deposition rate is 0.4 - 0.6 gm/min and the preform preparation process takes approximately 16 hours for a 0.30 NA preform, including tube cleaning, set up, collapse and removal from the lathe.

The preform is stored in a clean transfer container while awaiting fiber drawing, and one preform has been stored six months with no degradation of the 2.1 GPa prooftest yield.

2.3 Fiber Drawing

The preform is drawn to an optical fiber in the apparatus shown in Figures 4 and 5. The 4 meter drawing tower contains an absolute filter mounted at the top which provides laminar flow air to the preform. Periodic particle counts using a Royco particle counter in the vicinity of the puller indicate an average of 0-1 particles/ft^3 - min within the enclosure.

The ZrO_2 induction furnace is driven at 3.8 MHz to 2300°C (controlled to ± 1.0°C) by a Lepel RF generator, and is designed to provide a quiescent air atmosphere at the neckdown region while preventing any stray ZrO_2 particles from reaching the fiber. The fiber is drawn by a capstan and wound onto the 15 cm diameter take up drum at low tension.

The fiber is coated with 80 μm of thermally cured silicone as it is drawn, and the diameter of the uncoated and coated fiber is monitored by a pair of Lasermikes(TM). The upper Lasermike(TM) also controls the fiber diameter to ± 0.5 μm (one sigma value) at 140 μm by an HP 9825 calculator driven feedback loop to the capstan and to the preform drive.

All important process parameters are controlled and datalogged by the HP 9825 calculator including preform rate, fiber draw rate, ZrO_2 furnace temperature, silicone thickness and silicone cure temperature. A plot of the data generated during a typical run is shown in Figure 6.

The drawn fiber is then either characterized optically and mechanically as is, or it is coated with Hytrel(TM) to 1.0 mm diameter in a separate extrusion operation. The Hytrel(TM) extrusion is particularly useful for prooftesting at stresses greater than 0.7 GPa since the soft silicone jacket is easily abraded and torn by the rotating belts of the prooftester.

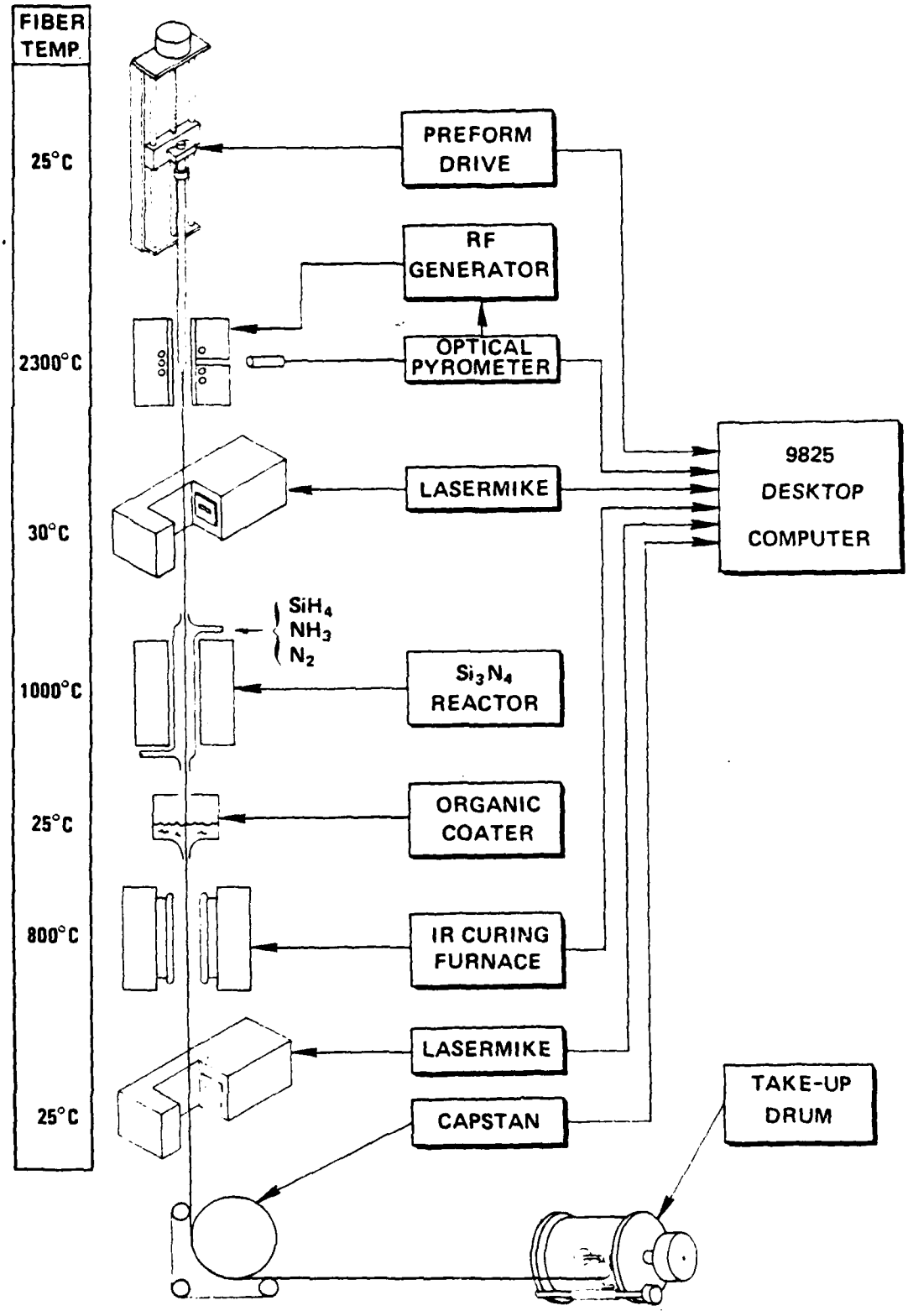

Figure 4. Schematic of the fiber puller.

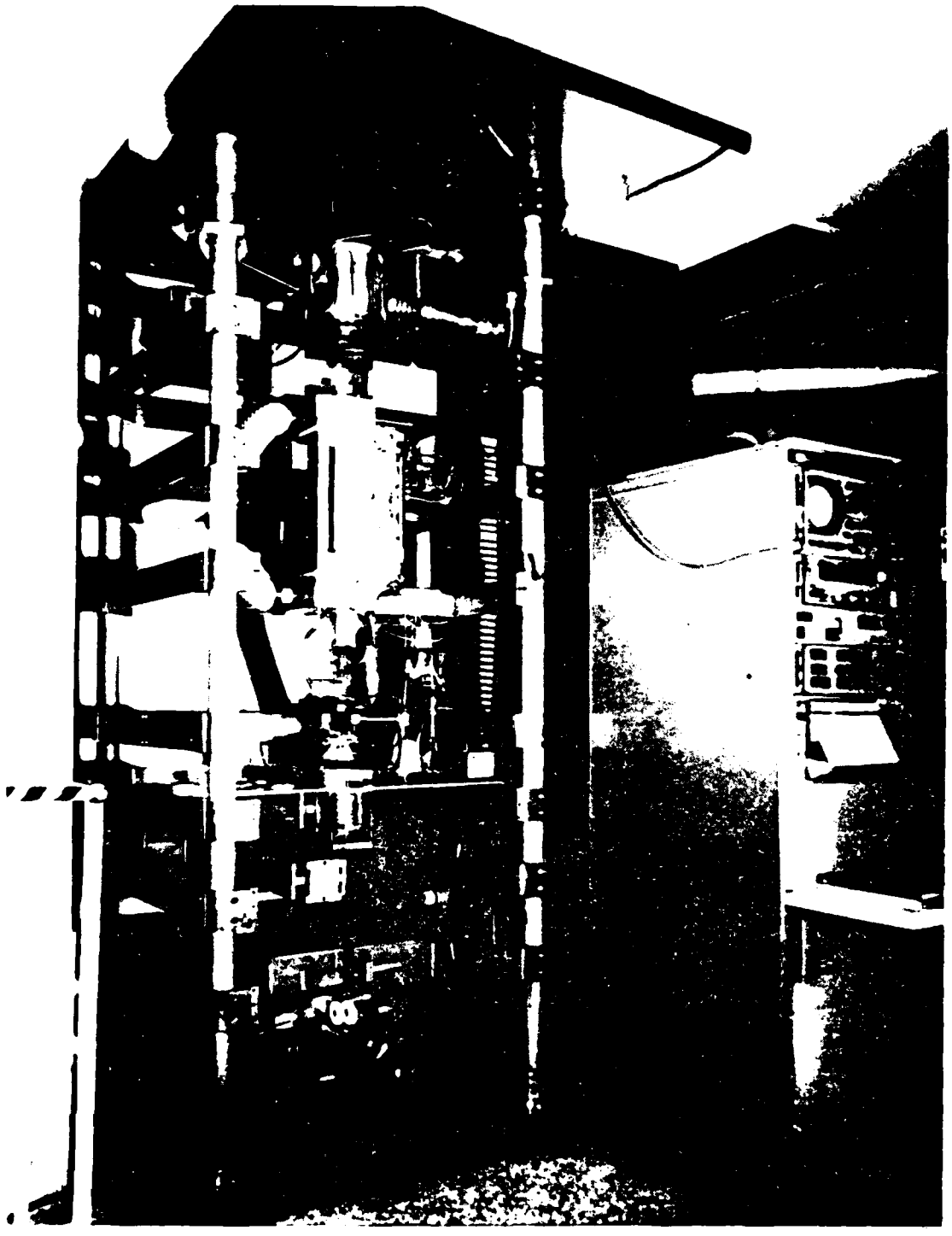

Figure 5. Optical Fiber Drawing Tower and Associated Electronics.

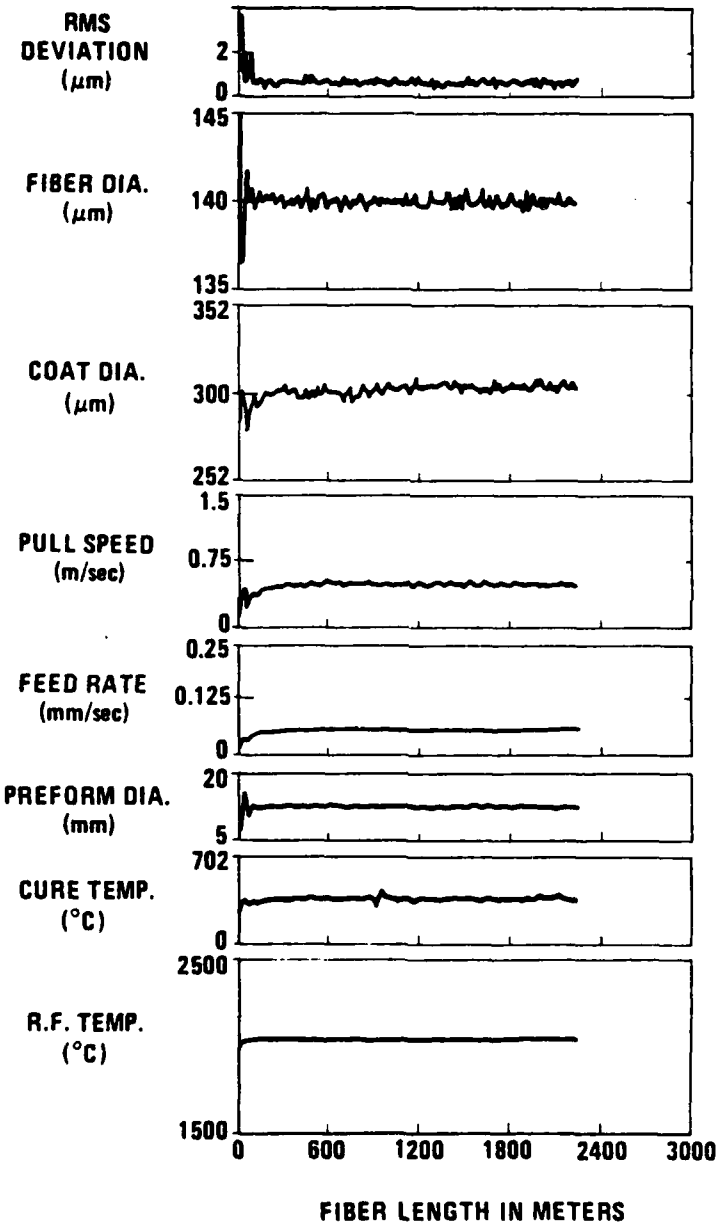

Figure 6. Data logged during a fiber draw.

2.4 Silicon Oxynitride Deposition

The silicon oxynitride reactor is placed just above the silicone coating cup for application of the thin fatigue resistant oxynitride film. Silane and ammonia in a diluent of nitrogen are introduced at one end of the heated reactor while exhaust gases and particulates exit the other end. The reactor operates at near atmospheric pressure with baffles and pressure differentials to exclude oxygen (which reacts preferentially with the silane to form SiO_2), and to keep any unreacted silane or ammonia from escaping. The silane and ammonia are kept in negative pressure gas vaults plumbed directly to vents on the roof of the building, and welded stainless steel piping is used throughout the system. Effluents from the oxynitride reactor are exhausted to the building scrubbing system which is capable of handling the usual array of toxic semiconductor wastes.

Appropriate laminar flow conditions are achieved inside the reactor (schematically shown in Figures 4 and 7) to minimize the chances of particulates formed in the homogeneous vapor phase reaction from sticking to the fiber and causing possible weak flaws.

The reaction proceeds in the absence of oxygen according to the approximate relation

$$3\ SiH_4 + 4\ NH_3 \longrightarrow Si_3N_4 + 12\ H_2. \qquad (1)$$

Silane starts to decompose at 500°C to form free silicon, and will also react spontaneously with atmospheres containing greater than 3% oxygen at room temperature. To exclude these unwanted side reactions, nitrogen is used as a diluent, keeping the partial pressure of silane below 5% in the reaction chamber and in the exhaust lines.

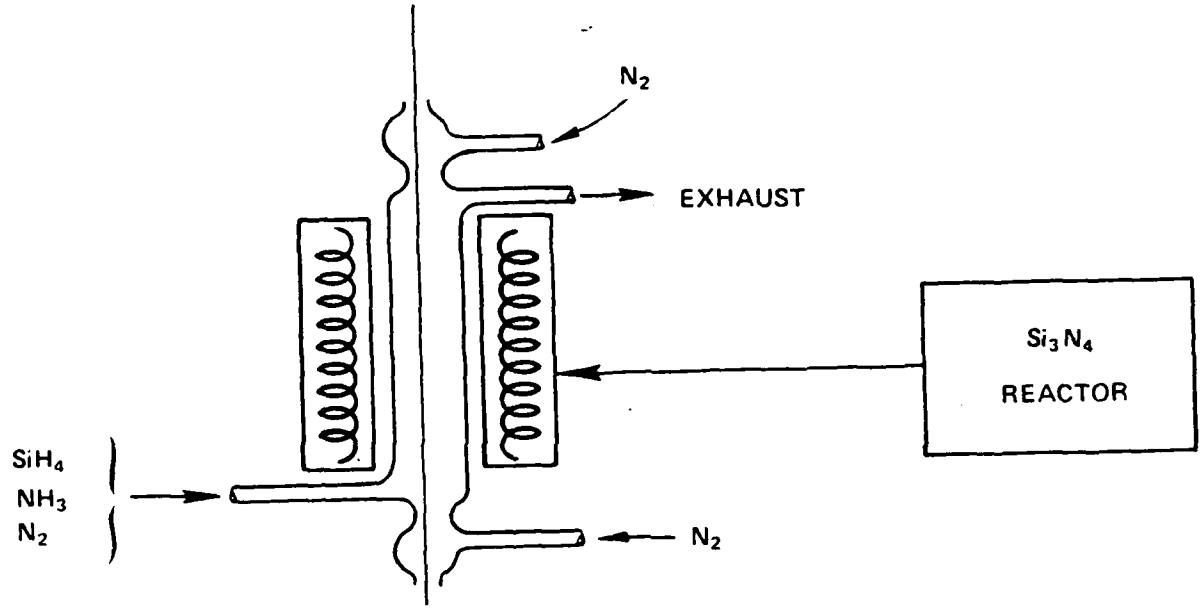

Figure 7. Silicon Oxynitride CVD Reactor.

Many intermediates are possible[6] in the overall reaction of Equation (1), but are not considered here. Equation (1) is only approximate because amorphous silicon oxynitride is not necessarily stoichiometric and is quite often found to be silicon rich unless large excesses of ammonia are present in the reactor.[7] Other significant constituents of the reaction products include hydrogen[8] (up to 20-25%) which can reside at atomic defects or broken bonds in the structure, and oxygen, which reduces the thermal expansion mismatch between silica and silicon oxynitride. Although reaction (1) can proceed by a variety of mechanisms including thermal activation,[9] plasma assisted activation[10] or photoactivation,[11] only the thermally activated, high temperature, atmospheric pressure, pyrolytic reaction mechanism has been used during this phase of the research, primarily because of the high deposition rate (exceeding 1000 Å/s) required to make the online application of a sufficiently thick coating a practical low cost process.

In addition to silane and ammonia, there are a variety of possible starting materials for the reaction, including $SiCl_4 + NH_3$, $SiF_4 + NH_3$, $SiH_4 + N_2H_4$, and $SiHCl_3 + NH_2$.[12] We have chosen $SiH_4 + NH_3$ because of our experience in pyrolytic deposition of high quality films of silicon nitride in semiconductor operations using this reaction.

A variety of experiments utilizing different reactor designs were carried out to develop the presently used silicon oxynitride deposition process. The current process is capable of continuously coating multi kilometer fibers with a fatigue resistant particulate free silicon oxynitride film, yielding fibers with mean strengths of 2.8 GPa.

3.0 Silicon Oxynitride Characterization

The silicon oxynitride films have been characterized by a variety of direct techniques, including Auger analysis to determine composition and thickness, scanning electron microscopy to examine surface morphology, and selective etching studies coupled with both optical and electron microscopy. Results of these direct characterization techniques will be presented here, while the results of indirect studies such as strength and fatigue measurements will be discussed in later sections.

3.1 Auger Analysis

Auger Electron Spectroscopy combined with ion milling has provided us with valuable information concerning the approximate stoichiometry and thickness of the silicon oxynitride films. The hardware used includes a Varian single pass CME with a 0.3% energy resolution and an integral electron gun which produces a < 5 μm diameter electron beam at energies between 100 eV and 10 keV. Sputtering is accomplished using a Perkin Elmer differentially pumped ion gun. The system is controlled and the data is processed with an HP 1000F minicomputer.

The standard experimental conditions involve a 2 kV electron beam at a current of 0.63 microamp. The differentially pumped ion gun is run at 2 kV with a 1 mm square raster; the system pressure is typically in the low 10^{-7} Torr range. Standard peak shapes are recorded and sensitivity factors are calculated for each profile.[13,14] Spectra for the depth profiles are taken at discrete depths called cycles every 10 - 20 angstroms with 1 eV data steps. Sputter rates on standard thickness oxides are typically 60 A/min.

Sample preparation has been designed to minimize the problem of sample charging. A small region of the fiber is masked while the rest is sputter coated with gold. The fiber is mounted on a 30° tray in the plane containing the axis of the electron beam and the sample normal. A plot of film composition versus depth for a particular fiber is shown in Fig. 8. The film composition at the nitrogen peak is $SiO_{.42}N_{1.36}$. This nitrogen peak occurs at a depth of 150 Å from the film surface. The film shows a graded composition tending towards SiO_2 as the original fiber surface is approached at ~ 450 Å depth. The repeatability of the technique has been checked by repeated analysis of adjacent sections of the same fiber and

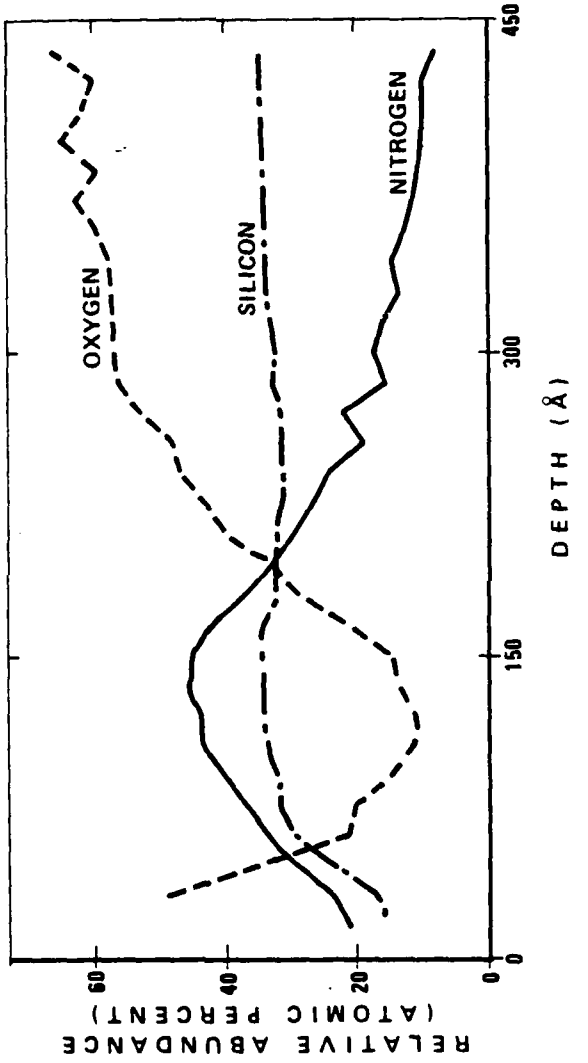

Figure 8. Auger depth profile of silicon oxynitride coated fiber no. 1252.

is estimated to be $\pm$ 5% in composition and $\pm$ 50 Å in depth. The quantitative accuracy of the technique is harder to estimate since comparison with known composition standards of a different (flat) geometry is involved.

However, the composition of the fiber under the silicon oxynitride film should of course be very nearly SiO_2, and therefore, the data can be normalized by ion milling completely through the film. This was done in Fig. 8. An additional limitation of the technique is that the apparent "grading" in the stoichiometry may be due in part to broadening caused by non-uniform ion milling and other effects due to the small cylindrical geometry of the fiber. Nevertheless, Auger spectroscopy has provided valuable insights for optimization of the film properties.

3.2 Surface Morphology

It is generally recognized that fiber surface morphology plays a primary role in determining fiber strength. Intrinsic strength is limited by the presence of surface flaws, which can be generated by a variety of mechanisms including stress caused by the presence of a foreign particle on the pristine fiber surface. Such contamination can arise from dust particles in the environment, or in our case, silicon oxynitride particles formed spontaneously in the vapor phase inside the silicon oxynitride reactor. Since it is difficult to stop this homogeneous vapor phase reaction from occurring, it is essential to keep such particulates away from the fiber surface by appropriate reactor design and reactant flow conditions.

Although particulate contamination ultimately manifests itself as a large number of weak flaws, as determined for example by prooftesting, it can also be monitored directly by scanning electron microscopy (SEM) of selected portions of the fiber surface. Some examples are shown in Figures 9 - 12. Morphologies shown in Figures 9 - 11 (typical results from our early experiments) are correlated with numerous weak flaws at tensile stresses greater than 0.6 GPa. The smooth morphology shown in Fig. 12, achieved with our current process, results in long fiber lengths with a minimum strength greater than 2.1 GPa. The flocculates in Figures 9 - 11 appear to cover a thin continuous film of silicon oxynitride even though the overlying deposits are themselves discontinuous. This observation is evidenced by the fact that the dynamic fatigue resistance of these fibers was quite high even though there were large numbers of weak flaws.[15]

In all of the SEM observations to date, there has been no evidence of any pinhole formation or discontinuous silicon oxynitride coatings. Absence of pinholes is supported by an abundance of indirect evidence such as dynamic and static fatigue measurements (see Section 4).

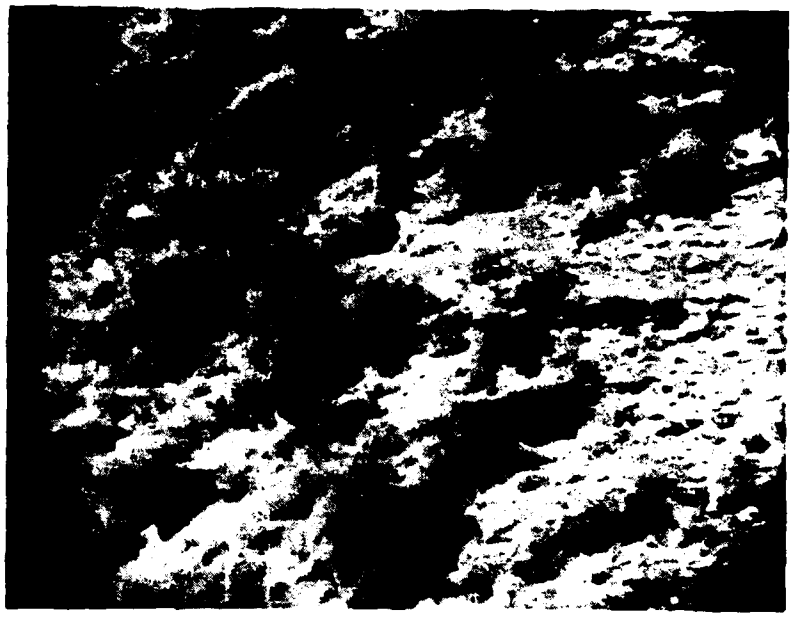

Figure 9. SEM photo of silicon oxynitride deposited on an optical fiber at 1000°C reactor temperature (10,000 X).

Figure 10. SEM photo of silicon oxynitride deposited on an optical fiber at 1100°C (10,000 X).

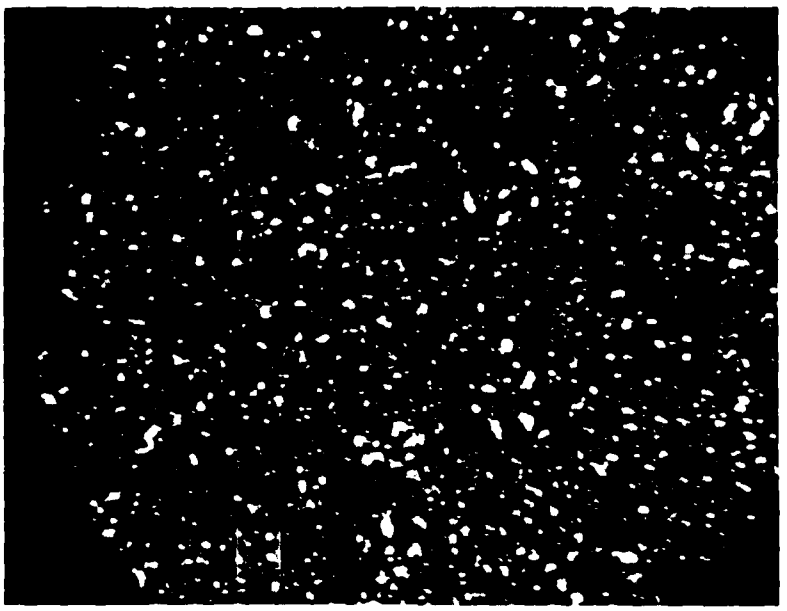

Figure 11. SEM photo of silicon oxynitride deposited on an optical fiber at 800°C (10,000 X).

Figure 12. SEM photo of featureless silicon oxynitride film deposited on an optical fiber at 1100°C (1000 X). The film is also featureless at 10,000 X.

The high Weibull slopes obtained in tensile strength measurements, indicative of extremely uniform strength along long lengths of fiber, and the high correlation coefficients obtained in the dynamic fatigue studies preclude the presence of pinholes in the silicon oxynitride films.

3.3 Etching Studies

Etching experiments have been performed, consisting of oxynitrided and non-oxynitrided fibers etched for varying lengths of time in HF. Surface morphology of these fibers etched for 0, 10, and 20 s in 24°C HF is shown in the SEM photographs in Figures 13 - 15. The non-oxynitrided fibers etch very smoothly in HF, but the oxynitrided fibers develop instabilities leading to a roughened surface, which persists even after the acid has etched completely through the film. The unstable morphology is consistent with the graded film composition discussed in Section 3.1 (ranging from pure SiO_2 at the inner surface to nearly stoichiometric silicon nitride at the outer surface) coupled with an order of magnitude greater etch rate for SiO_2.[12] Any surface perturbation that does develop is inherently unstable and leads to the morphologies shown.

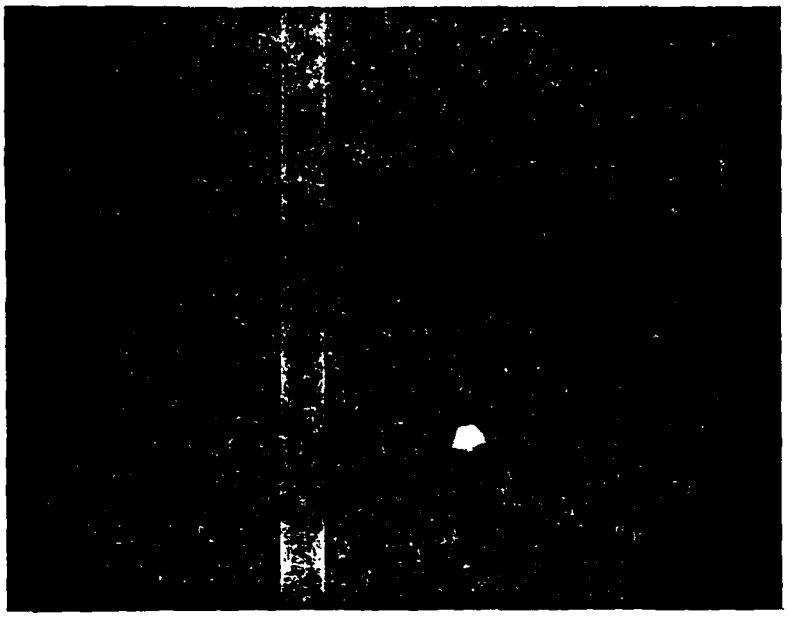

Figure 13. SEM photo of oxynitrided fiber (10,000 X).

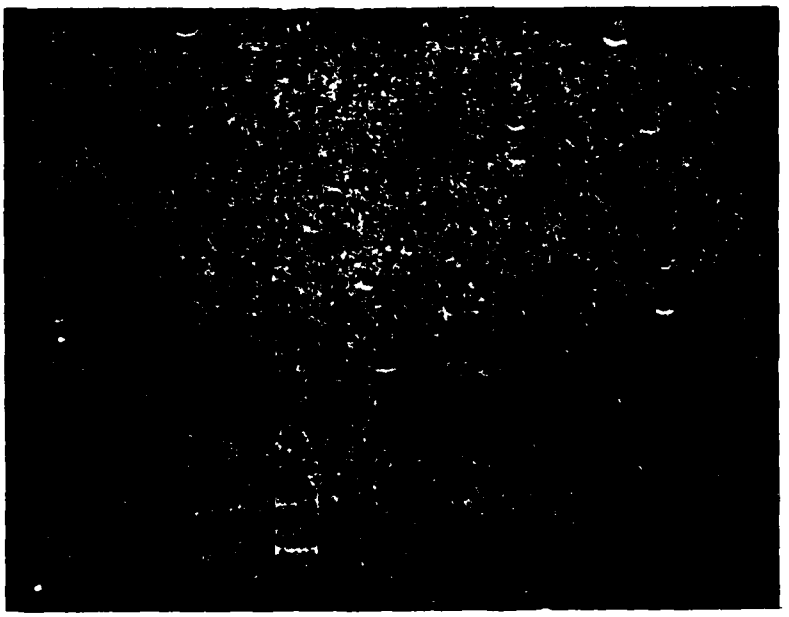

Figure 14. SEM photo of oxynitrided fiber after 10 s in HF (10,000 X).

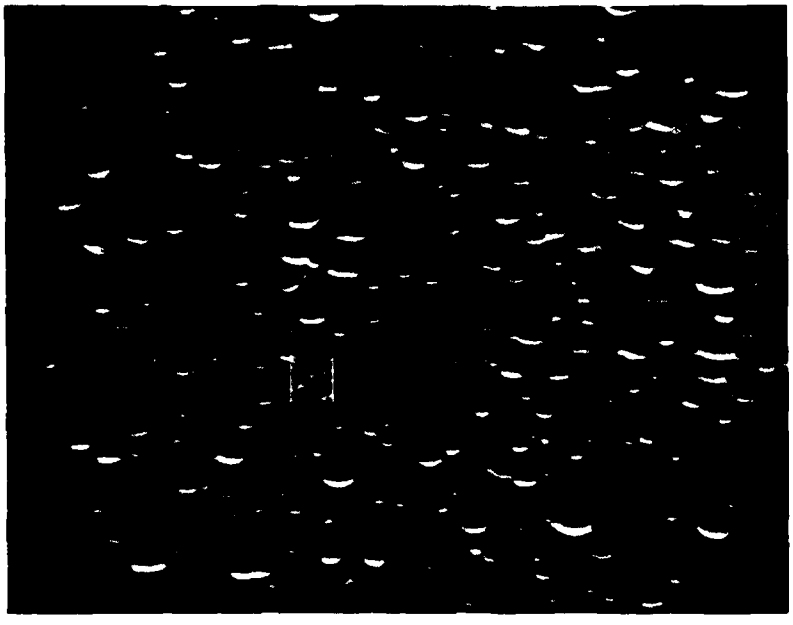

Figure 15. SEM photo of oxynitrided fiber after 20 s in HF (10,000 X).

4.0 Fiber Strength

4.1 Intrinsic Strength of Optical Fibers

It is well established theoretically that the intrinsic strength of pristine silica fiber is quite high, approaching 14 GPa.[16] This is supported by the Griffith crack model[17] and by actual tensile strength measurements in inert atmospheres.[18] However, the measured tensile strength of our silicon oxynitride fibers is much lower than the intrinsic strength, even in inert atmospheres, and lies in the range 2.8 - 3.5 GPa. Although the cause of the strength reduction compared to a non-nitrided fiber is not completely understood, there are a number of possible mechanisms which have been suggested. These are discussed in detail below:

(1) The silicon oxynitride film is already in tension because of the thermal expansion mismatch between silicon oxynitride and silica.

(2) The silicon oxynitride could somehow uniformly abrade the silica surface during initial stages of deposition.

(3) The silicon oxynitride film could exhibit an intrinsic tensile stress (present even at the deposition temperature).

(4) There could exist a uniform distribution of tiny pinholes which act as stress raisers.

(5) The tensile strength of silicon oxynitride could be less than that of SiO_2.

It can be demonstrated by the following analysis that thermal expansion mismatch contributes only a small portion of the observed strength reduction.

A force balance requires

$$\sum_i \sigma_i A_i = 0 = \sum_i (\varepsilon - \alpha_i \Delta T) A_i E_i \ , \qquad (5)$$

where σ_i = axial stress in i^{th} layer,

A_i = cross sectional area,

E_i = Young's Modulus,

α_i = thermal expansion coefficient,

ε = strain.

Now,

$$\alpha_{net} = \frac{\varepsilon}{\Delta T} = \frac{\sum_i A_i E_i \alpha_i}{\sum_i A_i E_i} \ . \qquad (6)$$

For HPL fiber (100 μm/140 μm core/clad, NA = .30), the materials constants are estimated as follows:

SiO_2 cladding: $E_o = 72.3$ GPa

$\alpha = 0.55 \times 10^{-6}/^\circ C$

$A = \frac{\pi}{4}\left[(140\ \mu m)^2 - (100\ \mu m)^2\right]$

GeO_2/SiO_2 core: $\alpha = 3.0 \times 10^{-6}/^\circ C$

$E_o = 61.1$ GPa*

$A = \frac{\pi}{4}(100\ \mu m)^2$

---

*From Ref.(19), NA = .36, E_o (.435) + (72.3 GPa)(.565) = 65.3 GPa, therefore E_o = 56.2 GPa. For our fiber, NA = .30 and doping will be smaller by the ratio $\left(\frac{.30}{.36}\right)^2$ = .694. Therefore, E_o = 72.3 GPa - (.694)(72.3 GPa - 56.2 GPa) = 61.1 GPa.

Substitution of these values into Eq. (6) yields

$$\alpha_{net} = \frac{(1.0)(72.3)(0.55 \times 10^{-6}) + (.96)(61.1)(3.0 \times 10^{-6})}{(1.0)(72.3) + (.96)(61.1)}$$

or

$$\alpha_{net} = 1.65 \times 10^{-6}/^{\circ} C.$$

Assuming a value for the thermal expansion coefficient of a thin amorphous silicon nitride film to be $\alpha = 3 \times 10^{-6}/^{\circ} C$[12], the strain in the nitride layer is

$$\varepsilon = (3 - 1.65) \times 10^{-6}/^{\circ} C \times 1000^{\circ} C = 1.35 \times 10^{-3} \text{ (tensile)}.$$

This is the strain which would be produced by an axial tensile stress applied to the fiber of $(1.35 \times 10^{-3})[(72.3 \text{ GPa} = 61.1 \text{ GPa})/2] = 0.09$ GPa.

Thus, the calculated thermal expansion mismatch for a deposition temperature $\sim$1000° C accounts for less than 0.1 GPa of the total strength reduction of 2.1 - 2.8 GPa between nitrided and non-nitrided fibers.

The hypotheses of uniform abrasion or a uniform and ubiquitous distribution of tiny pinholes are both unlikely, but the etching results obtained in Section 3.3 could be explained by pinholes as well as the unstable etching theory proposed in 3.3. However, the presence of pinholes appears inconsistent with the excellent fatigue resistance of these fibers (see Section 4.4).

The intrinsic tensile strength of silicon oxynitride is believed to be comparable to silica since the Griffith analysis predicts an intrinsic strength proportional to Young's Modulus, and reported values of Young's Modulus for silicon nitride are comparable to or higher than silica.[20]

The most likely explanation for the uniform strength reduction of silicon oxynitride coated fibers is the existance of an intrinsic tensile stress developed in the film during deposition. The semiconductor and thin film literature is replete with references to intrinsic stresses in thin films which can arise from a variety of causes.[21] A plausible model for the case of amorphous silicon oxynitride films on optical fibers consists of a nonequilibrium atomic arrangement in the film caused by the extremely rapid deposition rate exceeding 1000 Å/s. If the film grows layer by layer, each successive surface layer is covered up within 10 ms. The structure and equilibrium configuration of a surface layer certainly differs from that of the bulk, since (1) surface atoms have missing bonds at the free surface and (2) the surface layer can contain many missing atoms. If this surface configuration is frozen in by the rapid deposition rate, the resultant defect structure in the bulk contains a distribution of atoms separated by more than their minimum free energy separation, and the resultant increase in energy manifests itself in tensile strain.

4.2 Weak Flaws

Long lengths of strong fiber require the detection and elimination of the sources of weak flaws. There are a number of possible sources and we have taken a variety of steps to eliminate them.

It is well established that preform defects, including bubbles, inclusions, scratches and surface particles will be perpetuated during fiber drawing and cause weak points in the resulting fiber. It is, of course, important to maintain a clean environment around the preform operation and to use appropriate torch tip design to prevent any introduction of contaminants. The preform is transported to the drawing tower in a protective environment and thus is kept as clean as possible up until the actual drawing stage.

One of the most important diagnostic tools for determining the source of weak fiber flaws is fracture surface analysis. The ends of fibers which fail during tensile testing are saved and examined in a scanning electron microscope (SEM). This examination can reveal the location of fracture initiation. Through the use of the X-ray microprobe attachment to the SEM, the chemical composition of the region around the fracture initiation site can be examined.

Figure 16 shows a typical fracture surface which originates from a weak (< 1.4 GPa) failure. A smooth semi-circular "mirror" region is surrounded by a "mist" region and then a very rough "hackle" region. The entire pattern appears to radiate from a point on the side of the fiber in the center of the mirror region. Studies of fracture in glass samples having surface stress raisers at known locations have shown[22] that the fracture is actually initiated at the point from which the pattern appears to radiate. These studies

Figure 16. SEM photo of a fracture surface originating from a 0.35 GPa flaw.

have also shown that the mirror radius r_m and the strength s are related by:

$$S\, r_m^{1/2} = A \quad , \tag{7}$$

where A is a constant for any given type of glass. For SiO_2, $A = 2.23\ \text{MPa}\ m^{1/2}$.(22) In addition, it has been found that for large semicircular flaws (≥ 50 μm radius) in glass samples several millimeters across, the mirror radius is linearly proportional to the flaw radius r_o. For SiO_2, the mirror is 12.5 times larger than the flaw, so that

$$S\, r_o^{1/2} = 0.283\ A \quad . \tag{8}$$

For a flaw having strength S = 2.1 GPa, Equation 8 predicts that the flaw radius is 90 nm. If the strength is 0.7 GPa, the flaw radius is predicted to be 810 nm.

Fractures with mirror surfaces originating at the edge of the fiber, like those in Figure 16 , are by far the most common type of fracture. In some cases, additional features can be seen which give further clues to the origin of the fracture. For example, in Figure 17 , we show a fracture surface with a surface-originating mirror surface. In contrast to the fractures discussed above, however, this fracture surface shows a long scratch containing an embedded particle right at the fracture origin. The particle was examined by X-ray microprobe analysis and found to contain Zr. The flaw may have been caused by the impact of this particle on the hot zone of the fiber inside the ZrO_2 susceptor in the fiber drawing tower. The depression produced by the particle would lengthen into a "scratch" as the fiber lengthened by > 10,000 in pulling.

Figure 18 shows a much less common type of fracture surface with

Figure 17 SEM photo of scratch at origin of .35 GPa prooftest break (500 X).

Figure 18. SEM photo of a weak flaw caused by porosity in the fiber which generated a 2.1 GPa prooftest break (20,000 X).

voids present at the origins of the fracture. Another uncommon type is shown in Figure 19, where the mirror surface appears to originate in the bulk of the fiber. In this case, microprobe examination indicated Zr and Ce at the point of origin. These contaminants may be present as inclusions in the natural quartz substrate tubes. Figure 20 depicts a type of fracture frequently encountered in proof test breaks at 1.4 - 2.1 GPa (203-304 kpsi). This surface appears to be completely shattered, and there is no symmetrical mirror and hackle pattern to indicate the origin of the fracture. It is likely that this surface is not even the original fracture surface but rather an underlying surface exposed when the end of the fracturing fiber shattered into pieces.

One major source of possible contamination in the drawing process is the zirconia furnace, and about 30% of the 0.35 GPa proof-test breaks early in this research were correlated with ZrO_2 particles. The yttria stabilized zirconia is suspect because it undergoes a phase transformation in the range 1400°C - 1600°C. Portions of the inside surface of the ZrO_2 susceptor were examined by SEM, and a variety of potentially damaging features can be seen in Figures 21 - 23. Figure 21 shows the as-received ZrO_2 tube covered with loose particles. The same surface is shown in Fig. 22 after thorough washing. The loose particles are gone and the only surface features visible are small crystallites embedded throughout the grain. However, after one thousand hours of operation at an average temperature of 2000°C, the crystallites appear to be larger (as shown in Fig. 23) and more loosely attached to the surface. In addition, there are visible pores in the surface, which may have contained crystallites that were dislodged.

Figure 19. SEM photo of an inclusion just inside the edge of the fiber which caused a 1.4 GPa prooftest break (2000 X).

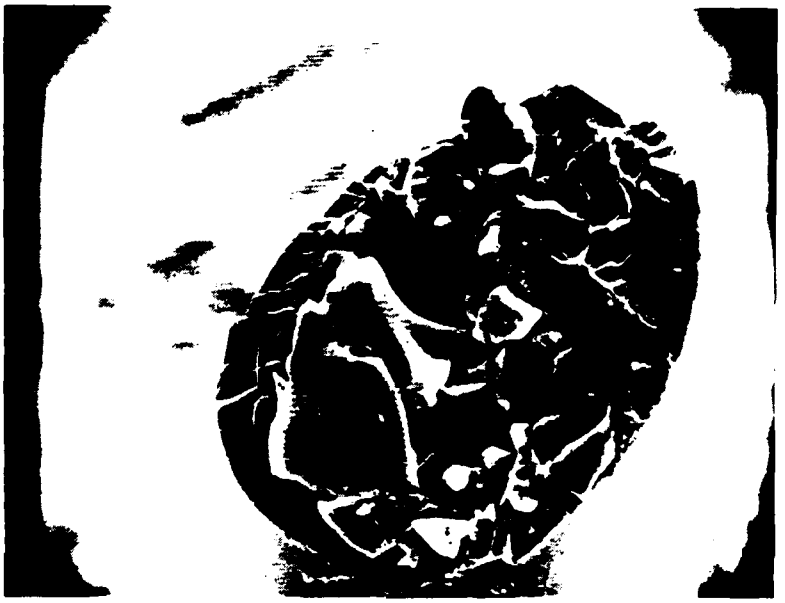

Figure 20. SEM photo of shattered surface of fiber fractured at a stress 1.4 GPa.

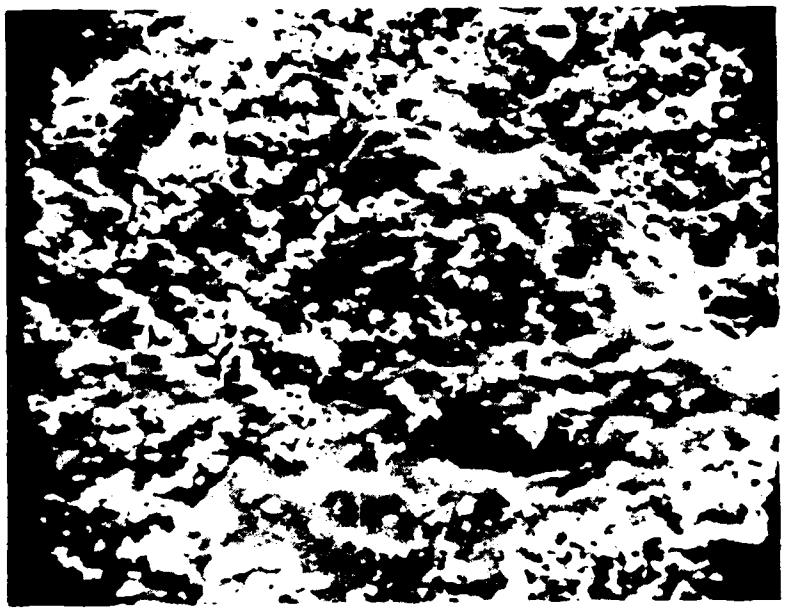

Figure 21. As-received ZrO_2 furnace tube (1000 X).

Figure 22. ZrO_2 furnace tube after washing (5000 X).

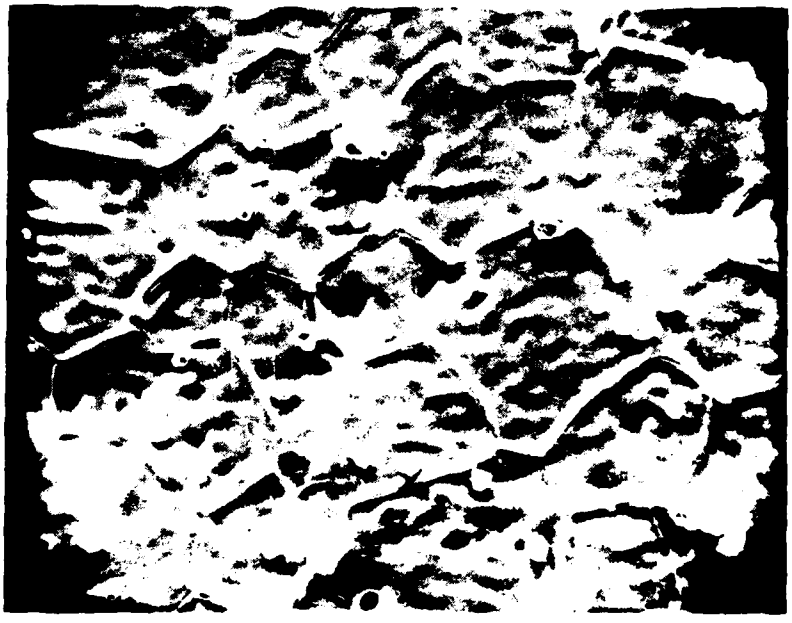

Figure 23. ZrO_2 furnace tube after one thousand hours at 2000°C (200 X).

We believe these dislodged crystallites may be responsible for the weak flaws, and have pursued two paths to reduce this potential source of contamination:

(1) investigation of ZrO_2 surface treatments including scrubbing, etching and polishing to clean the surface.

(2) design of an improved ZrO_2 furnace with appropriate pressure gradients to prevent loose particles from reaching the fiber surface.

Implementation of the new furnace design has dramatically reduced the incidence of 2.1 GPa prooftest breaks as discussed in Section 4.

The cleanliness of the fiber is also quite important, as experiments have shown[23] that particulate contact with the fiber before it is coated can substantially degrade its strength through the creation of flaws. In our drawing tower, the fiber enters a protective sleeve above the silicon oxynitride reactor immediately below the hot zone. Only a short length of fiber (< 1 cm) is exposed to ambient conditions. Again, upon leaving the reactor, the fiber is enclosed, protecting it from any particulates in the atmosphere until it is coated. There are particulates formed in the reactor (discussed in Section 3.2), but aside from these reactor-created particles, the fiber surface is well protected.

A correlation between fiber drawing tension and flaw density has been previously documented.[24] Fibers drawn at low temperature with tension > 10 grams have a significantly higher density of weak flaws (strength < 4 GPa) than fibers drawn at higher temperature and lower tension. The physical mechanism is most likely the incomplete healing of preform flaws in the hot zone resulting from the higher glass viscosity present during higher tension drawing. In our puller, the tension has been measured

to be 10 - 30 grams below the coating cup using a hand-held Tensitron(TM) gauge. The tension is less in the drawing region above the coating cup, but has not yet been measured.

After drawing, the silicone coated fiber is kept once again in a clean environment until it can be coated with a further protective jacket of Hytrel.(TM) An additional experimentally determined cause of weak (< 2.1 GPa) flaws is nonuniformity of the silicone coating, which results in occasional thin spots in the silicone and also leads to bumps in the Hytrel.(TM) By appropriate modification of the silicone coating cup, the frequency of thin spots in the silicone was reduced from one every 1 - 10 meters to less than one every 300 meters. Table II summarizes the prooftest yield of silicon oxynitride coated fibers fabricated with and without the improved silicone flow conditions. Further work is in progress to locate the causes of the weak points which still remain. This research is directed toward three main approaches: (1) correlation of proof test yield with fabrication conditions, (2) correlation of specific break locations with the locations of fabrication anomalies, (3) and continuing analysis of fracture surfaces.

Table II. Yield of silicon oxynitride coated fibers prooftested at 2.1 GPa (304 kpsi).

	Fiber Fabricated with standard silicone coater (open cup)	Fiber fabricated with improved silicone coater (shorter meniscus)
Total length proof tested	2811	21150
Longest piece surviving test	432	1349
Cumulative yield* $\geq$ 400 m	432	14266
Cumulative yield* $\geq$ 800 m	0	9620
Cumulative yield* $\geq$ 1200 m	0	3821

*Cumulative yield is defined as the cumulative length of all pieces surviving the proof test with an unbroken length longer than the stated length.

4.3 Experimental Mechanical Characterization Results

4.3.1 Instron Tensile Test

One of the principle instruments used in the HP optical fiber strength tests is an Instron Model 1122 Tensile Tester.[25] This machine (see Figure 24) is capable of testing short samples of fiber (up to 0.5 m guage length) at strain rates of $1.4 \times 10^{-6}\ s^{-1}$ to $2.8 \times 10^{-2}\ s^{-1}$.

This instrument is best suited to the precise determination of the mean failure strength and the distribution of failure strengths of ~0.5 m fiber samples. By performing tests at several strain rates, the fatigue properties of the fiber can be evaluated (see Section 4.4 for further discussion). Tests on this instrument also give information about the density of weak points along the fiber but only if long lengths of fiber (on the order of one km or more) are tested. Thorough evaluation of weak points with this machine is impractical because the rate of testing is only 150 m per working day. Such tests are better performed with the 20 m tensile tester or the proof tester (see below). The Instron can also be used for tests of fiber strength in a variety of environments and a variety of temperatures by installing an environmental chamber around the test section. However, this is cumbersome and such environmental and temperature-dependence tests are best performed with the bend tester (see below).

The Instron's strip chart records the load vs crosshead position during each tensile test. We compute the failure strength S_f

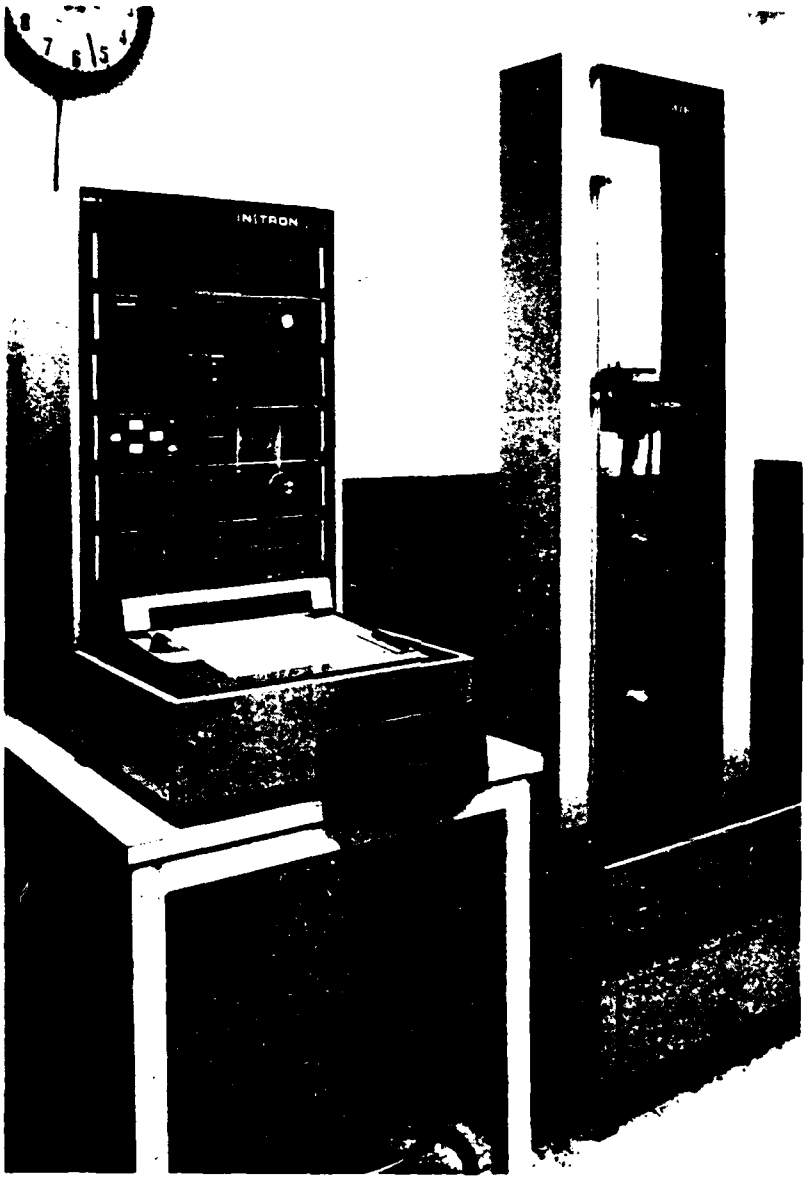

Figure 4. Instron Model 1122 Tensile Tester.

from the peak load at failure L_f using:

$$S_f = \frac{4\gamma L_f}{\pi d^2} \qquad (9)$$

where d is the fiber diameter and γ is the fraction of the load supported by the fiber. If the fiber is only coated with silicone and silicon oxynitride, $\gamma = 1$. If, however, the fiber has a coating of Hytrel over the silicone, we find that $\gamma = .96 \pm .02$. For the Hytrel coated fiber, we determine σ by monitoring the strain ε during the tensile test with a 50 mm gauge extensometer clipped to the fiber. We then use precision Bell Labs measurements[19] of $S(\varepsilon)$ to calculate S_f from ε_f.

To obtain quantitative strength values, it is important to take into account the statistical variation of the strength along the length of the fiber. Even though the strength of individual samples varies randomly, the mean strength of a series of samples will be nearly constant. The statistical distribution of fiber strengths can be well approximated by a Weibull distribution:[26]

$$F(S) = 1 - \exp\left[(S/S_o)^m\right] \qquad (10)$$

where S is the failure stress, F is the cumulative probability of failure at all stresses $\leq S$, and both m and S_o are constants for a given fiber. The constant m is called the Weibull slope. The standard deviation σ_s of the strength distribution satisfies

$$\sigma_s = 1.22 \frac{S_o}{m} \qquad (11)$$

For our fibers, the Weibull slope of the Instron data is typically 20-120, so that σ_s is 1% to 6% of S_o (see Figure 25). The mean strength of

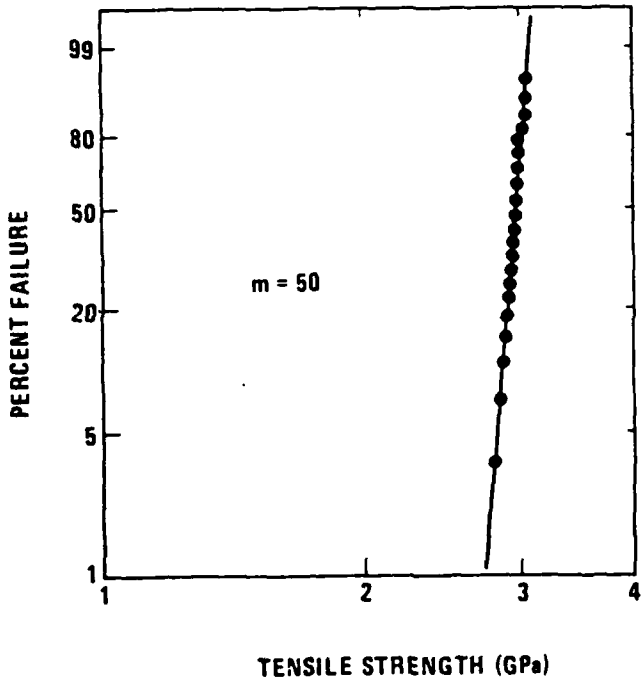

Figure 25. Typical data from Instron test of silicon oxynitride coated fiber.

tests of groups of N samples have a standard deviation about the mean of $\sigma_s/\sqrt{n}$. In our fiber testing program, each group of fibers contains N=25 samples. Therefore the mean strengths are accurate to a standard deviation of 0.25% to 1.25% of S_o, for an m of 20-120. The 95% confidence level ($\pm$ 2 standard deviations) is $\pm$ 0.5% to 2.5% of S_o.

In analyzing the Instron test data for any one group of fibers, we count only those samples which break between the two grips and not those which break on the grips. The small proportion of samples which break on the grips cannot be used for meaningful data because the stress is not precisely known in the gripped area. We then enter the data into the analysis program which graphs the data on Weibull probability axes (ln S vs ln ln $[1-F(S)]^{-1}$). This program uses a linear regression routine to compute a least squares fit to the data, and also to compute the coefficient of determination for the data. If the coefficient of determination is less than 0.70, the program automatically eliminates the lowest strength data point in the group and recomputes F(S). It then recomputes the least squares fit. If the coefficient of determination is still less than 0.70, the program eliminates the second lowest strength data point. If necessary, additional data points are eliminated from the lower end of the strength distribution until the coefficient of determination is >0.70. This procedure eliminates any strength points which belong to the lower strength mode if the distribution is bimodal. These points in the lower strength mode must be eliminated because they are not representative of the majority of the fiber and the number of them present in a group of 25 is typically only 0-1. The low number present in any group

results in a significant statistical variation in the contribution of these lower strength mode points to the overall mean strength of the group. A more meaningful mean strength, subject to less statistical variability, is obtained by omitting these points.

In Table III , we summarize the Instron strength results for a number of silicon oxynitride coated fibers. As discussed in Section 2.4 , the strength is affected by the composition of the films, so we list in Table III the partial pressures of the reactants NH_3 and SiH_4 plus that of the carrier N_2. This table also lists the mean strength of the fiber and its Weibull slope, both measured at 1000 mm/min on the Instron.

When only the carrier gas is present (e.g. #1253) there is no oxynitride coating deposition and the strength of the fiber is 5.0 GPa, the value for conventional fused silica fiber. With the normal reaction conditions (0.494/0.494/0.013 partial pressures), the strength is typically 2.8 GPa. When the reactant partial pressure is reduced by a factor of 3 from normal (e.g. #1251), the strength drops to 2.2 GPa. When the N_2 flow is off, the strength is 2.4-2.5 GPa for a NH_3/SiH_4 ratio of 42 (e.g. #1310) but 3.4 GPa for a NH_3/SiH_4 ratio of 80 (e.g. #1320).

The differing oxynitride coating compositions in this table also exhibit differing degrees of fatigue resistance. This aspect of the fiber strength is discussed in Section 4.4 . Optimization of the overall static fatigue performance must take into account both the mean strength and the fatigue resistance, and is discussed in Section 5.0.

4.3.2 20 Meter Tensile Test

A second instrument used in the HP optical fiber strength tests is the 20 m tensile tester. This machine (see Figure 26), designed and

Table III

Tensile strength of 140 μm diameter
Silicon oxynitride coated HP fibers.

Fiber No.	Partial Pressure N_2	NH_3	SiH_4	Mean Strength (GPa)	Weibull Slope (m)
1150	0	.978	.022	2.2	30
1170	.494	.494	.012	2.4	18
1240	.494	.494	.012	2.9	60
1251	.830	.166	.004	2.2	23
1252	.494	.494	.012	2.5	41
1253	1.00	0	0	5.0	31
1290	.494	.494	.012	2.5	62
1300	0	.977	.023	2.5	51
1310	0	.977	.023	2.4	37
1320	0	.987	.012	3.4	28
0040	.491	.491	.017	2.7	32
1570	.494	.494	.013	2.7	50
1600	.494	.494	.013	2.8	20
1601	.494	.494	.013	2.7	66
1631	.494	.494	.013	2.8	37
S120	.494	.494	.013	2.9	59
1610	.494	.494	.013	2.8	52

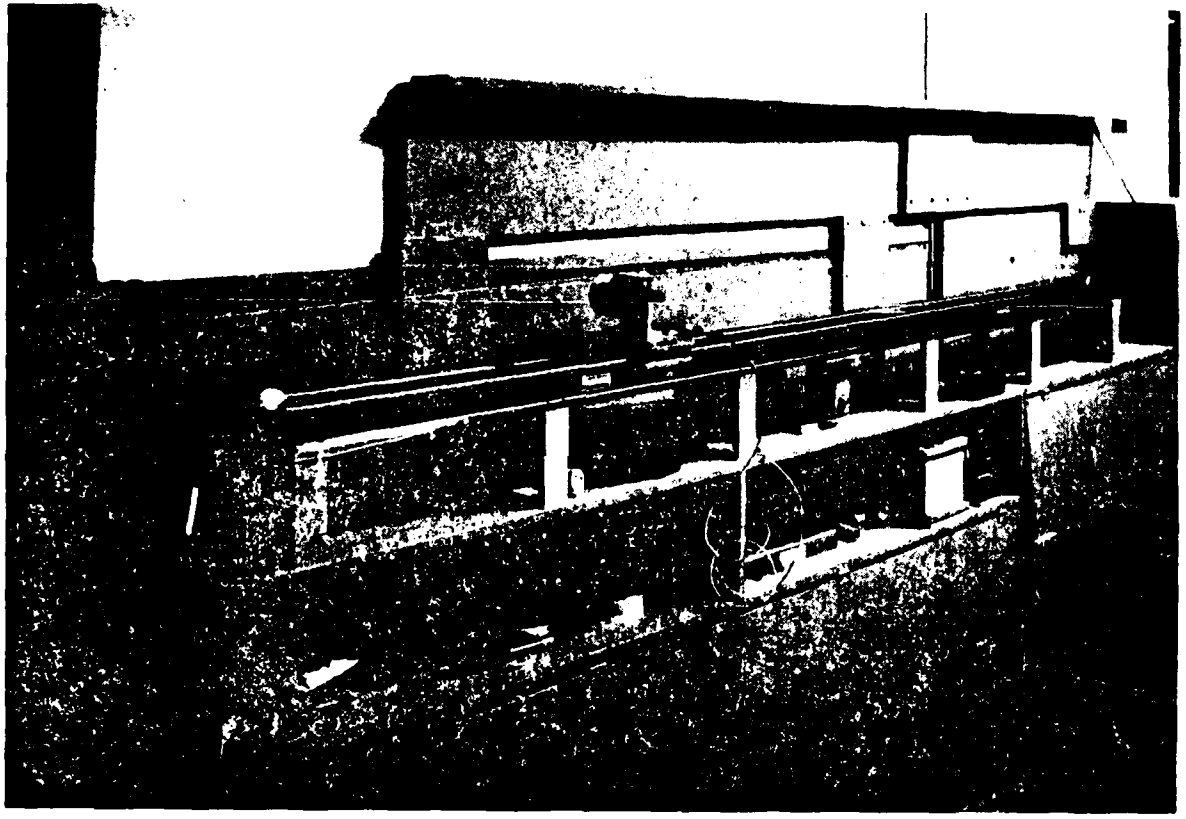

built in house, tests 20 m samples of fiber at strain rates up to $3.3 \times 10^{-3}\ s^{-1}$ (i.e. crosshead speeds up to 4000 mm/min). An electronic tension guage on the moving crosshead measures the load on the fiber (maximum load up to 100 N). The tension output is plotted on a strip chart recorder allowing determination of the failure stress using Equation 9.

This instrument is best suited to the determination of the statistical distribution of failure strengths of the weaker flaws in a fiber with a bimodal flaw distribution. The rate of testing is over 1 km per working day. The major disadvantage of this test is that it is a destructive test, with each 20 m sample being tested to failure. For this reason, testing of weak points is now conducted entirely with the proof tester (see below) which provides much of the same information in a non-destructive fashion. As discussed below in the section on prooftesting, cross comparison tests have been made which have shown excellent agreement between the prooftest data and the 20 m test data.

4.3.3 Proof Test

Our optical fiber strength tests rely on a continuous fiber prooftesting machine (see Figure 27) for evaluation of the distribution of weak points in fibers. This machine, designed and built in house, tests fibers at speeds up to 1.0 m/s at loads of 0 to 45 N (i.e. up to 3.0 GPa [=435 kpsi] for 140 μm fiber diameter). The fiber is wound from one reel onto a second reel, and is stressed between the two reels. The stressing is accomplished by passing the fiber through two drive capstans. The second drive capstan pulls the fiber faster than the first, so that the section of fiber between the capstans (1.0 m in length) is continuously

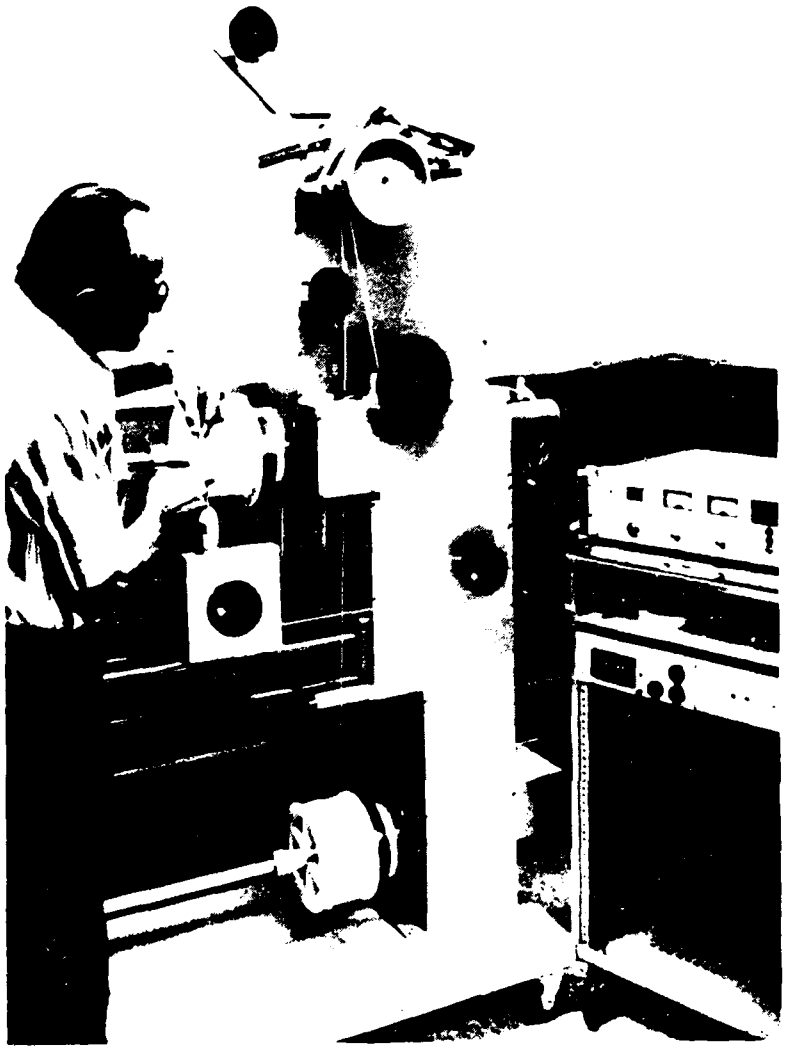

Figure 27. Proof tester for continuous tensile testing up to 45 N.

stressed. Between the two capstans, the fiber passes around a pulley mounted on an electronic Tensitron(TM) gauge which measures the fiber tension. The proof tester features a level-winding takeup mechanism, as well as a servoed takeup drive which maintains only 25 g fiber tension (i.e., a stress of 16 MPa) on the takeup reel. If the fiber breaks, the reduction in the Tensitron(TM) output automatically stops the machine.

Reduction in the minimum guaranteed strength could be caused by dynamic fatigue during the stress unloading, but our proof tester avoids this problem by using rapid stress unloading. For example, at 1 m/sec and $s = 0.70$ GPa, the unloading rate is $\dot{s} > 3.5$ GPa/s. This proof tester reliably tests the strength of Hytrel-jacketed fiber. We see no evidence of the creation of any new flaws by the proof tester. We have proof tested one 300 m section of fiber at 2.1 GPa for ten successive proof test runs without experiencing any failures. Also, we have used a different section of fiber and determined that the fiber failure probability follows the Weibull distribution. In this second test, the fiber was stressed in 9 proof test runs, each at a successively higher stress. After the completion of these tests the failure points were plotted on a Weibull graph (see Figure 28). Then the remaining fiber was tested to failure in our 20 m tensile tester (see above). The failure points from the two test machines all fell on a smooth curve, indicating that the proof tester had not measurably degraded the fiber strength distribution.

The fiber does need to be Hytrel(TM)-jacketed in order to be proof tested because the bare silicone layer would be damaged by the capstans. An exception is that tests up to 0.35 GPa can be performed on unjacketed fiber without damage. At these low stresses, the forces exerted by the capstans on the bare silicone are small enough that the silicone is undamaged. Table II (page 44) summarizes the proof test yield of recent silicon oxynitride fiber.

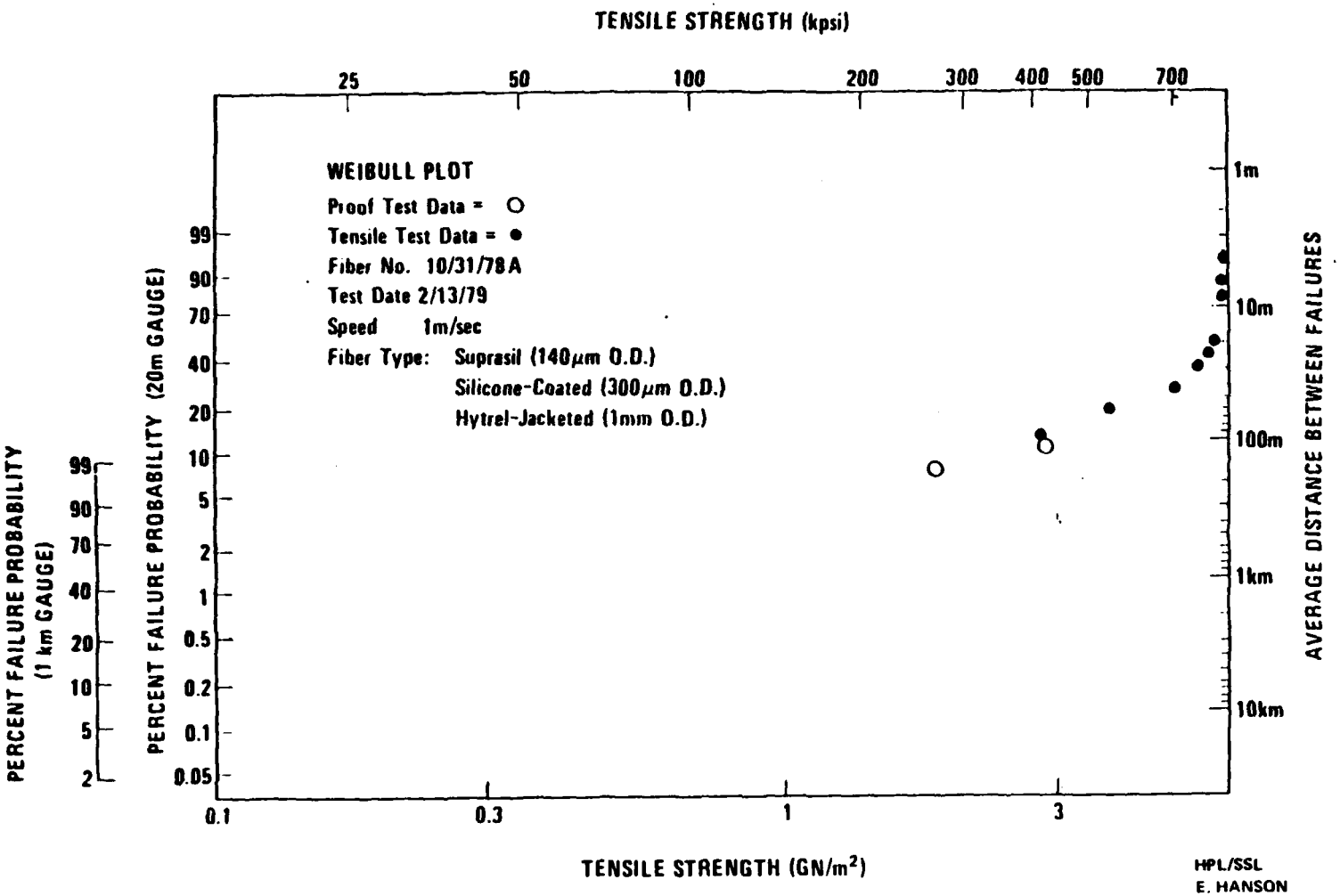

Figure 28. Weibull plot of the strength distribution in a non-oxynitride coated fiber tested first at 9 sequentially higher proof test levels and then tested in the horizontal tensile tester.

4.3.4 Bend Fracture Test

Another test instrument used in the HP optical fiber strength tests is the bend fracture tester. This is a small portable apparatus (see Fig. 29) designed and built at HP along the lines of the device described by France et al.[27] Sections of fiber are bent between two flat plates as the two plates are driven together at a constant velocity. The plate separation D at the moment each section of fiber fractures is recorded. From that separation, the radius of curvature R of the fiber at fracture and the strain ε on the outer surface of the fiber are calculated from

$$\varepsilon = \frac{d_f}{2R} \; ; \; R = 0.42 \; D \qquad (12)$$

where R is the radius of curvature and d_f is the fiber diameter. The stress on the outer surface is then deduced from the known relationship[19] between stress and strain.

The bend fracture tester is well suited to tests of fiber strength in a variety of environments and at a variety of temperatures (see below). It is also suitable for testing pieces of fiber after they have been aged or subjected to various environments because it can test 10 cm long pieces with a variety of coatings.

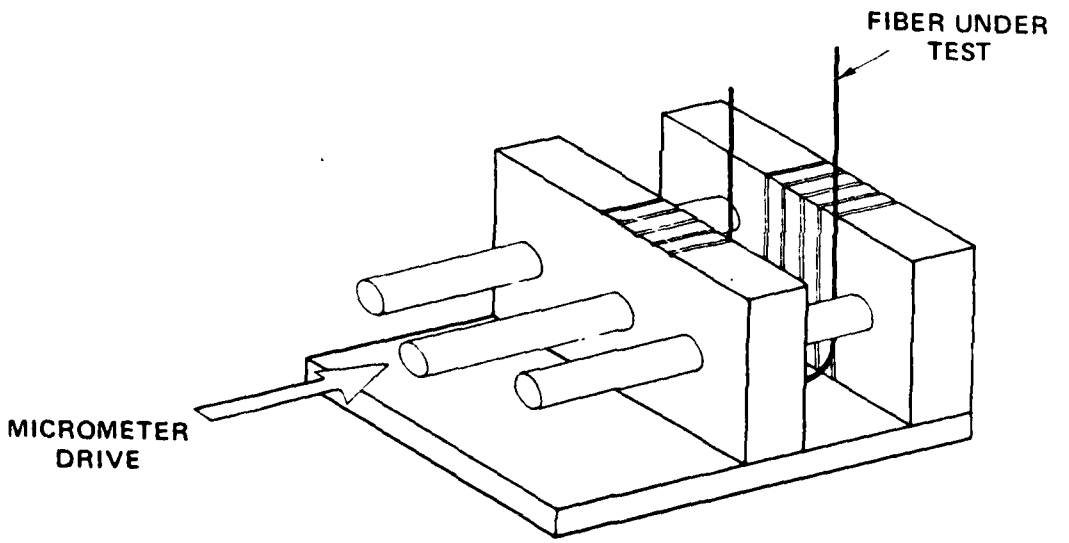

Figure 29. Bend Test Apparatus.

4.3.5 Temperature Effects

Using the bend fracture tester, we have performed tests on fibers at temperatures from -196°C to +200°C in environments including liquid nitrogen, acetone, ambient air, hot water, and silicone oil. Results to date are shown in Figure 30 . The conventional fiber increases substantially in strength as the temperature is decreased, and at liquid N_2 temperature its strength approaches the theoretical value predicted[28] for SiO_2. The large change in strength between ambient and liquid N_2 is a manifestation of the substantial stress corrosion present in SiO_2 fibers at ambient temperatures. In contrast, the silicon oxynitride coated fiber exhibits only a small temperature dependence. This is the behavior that would be expected for a fatigue resistant fiber.

Other features of the curves in Figure 30 include the slight rise in strength above ambient temperatures in silicone oil for the conventional fiber. This is in agreement with earlier Rolls Royce data[29] and is consistent with the hypothesis that there is less ambient moisture available at the fiber surface for stress corrosion at these temperatures. In contrast, tests performed in 95°C water show a significant strength reduction for the conventional fiber. For the silicon oxynitride coated fiber, they show only a slight reduction consistent with its higher fatigue resistance.

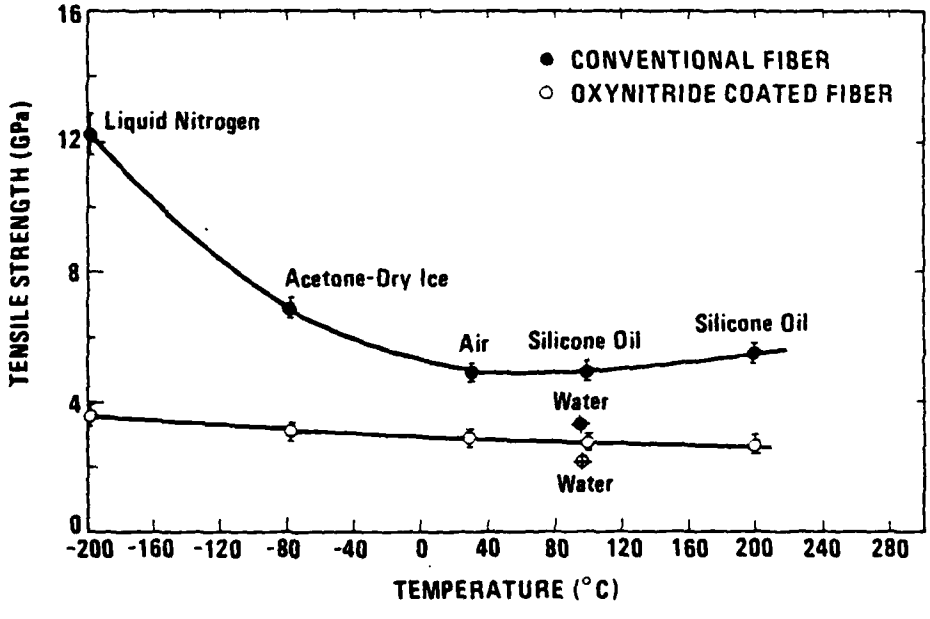

Figure 30. Strength measured in bend test as a function of temperature for fiber 1252 (oxynitrided) compared to a conventional (non-oxynitrided) fiber.

4.3.6 Aging Effects

Zero stress aging studies in water have also been initiated on both nitrided and non-nitrided fiber using the bend tester. To date, 0, 10, 100 and 1,000 hr aging tests have been completed. The data are shown in Figure 31, and indicate no reduction in strength upon aging for the non-nitrided fiber, in agreement with other observations[30]. The silicon oxynitride coated fiber, however, exhibits a very small reduction in strength with time, indicating clearly the presence of a different fracture mechanism in this type of fiber. The data indicate that a nitrided fiber with an initial fast fracture strength of 2.9 GPa will experience an extrapolated strength reduction of 14%, down to 2.5 GPa, after immersion in water for 100,000 hr. This reduction does not constitute a significant liability, and may actually provide useful diagnostic information about the stress corrosion and fracture phenomena in the nitride film.

We have determined that the decrease in strength of the silicon oxynitride coated fiber during stress-free aging is not caused by stress corrosion. The only way that stress corrosion could be responsible would be if a large tensile stress were present in the oxynitride film. For the fiber shown in Figure 31, the stress corrosion properties have been measured, and $u = .0078 \pm .0125$ (See Section 4). In order for stress corrosion to cause a measureable degradation, the intrinsic stress present in the film would have to be nearly equal to the strength of the film. However, the time dependence of strength would follow a curve very different in shape than that observed - it would be horizontal and then abruptly drop to zero. The aging in Figure 31 may well be a corrosion phenomenom but we conclude that it is not the type of stress-assisted corrosion responsible for static fatigue.

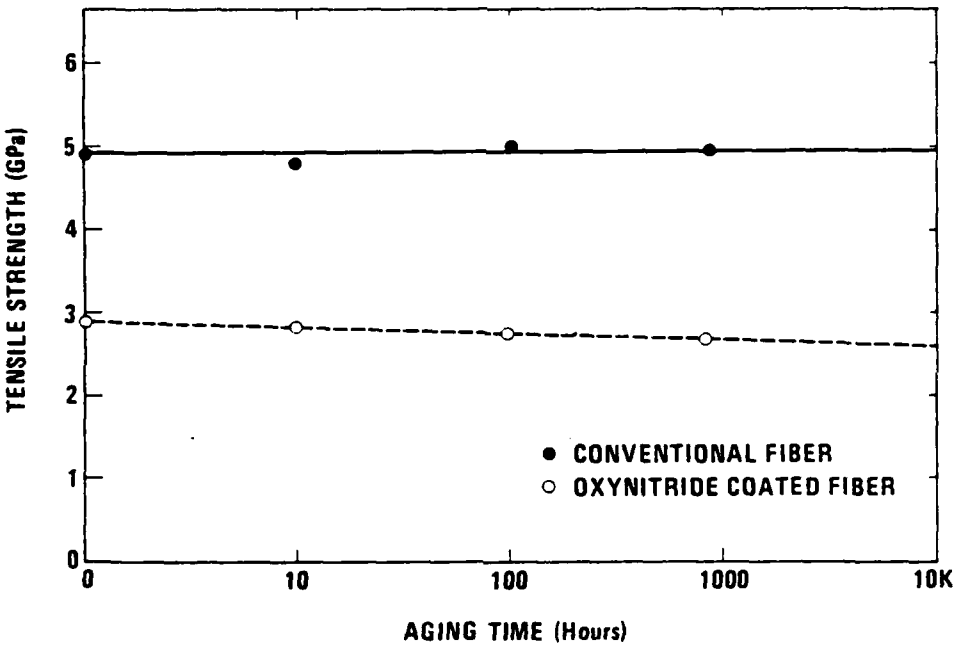

Figure 31. Strength measured in bend test after varying durations of zero-stress aging in 22°C deionized water.

5.0 Fiber Fatigue

5.1 *Introduction*

Fatigue in silica fibers has been shown to be caused by chemical reactions which break bonds in the lattice[29,31]. These bond breaking reactions only take place in the presence of three factors: tensile stress which stretches the lattice bonds, reacting species (such as OH^-, H^+ and Na^+), and a temperature high enough to produce an appreciable reaction rate. Ambient temperatures and ambient H_2O concentrations (at 30 - 80% R.H.) are high enough to produce appreciable reaction rates and subsequent stress corrosion.

As will be discussed further below, the static fatigue caused by stress corrosion in conventional fiber requires a reduced allowable service stress (for 10 year service life) of only 39% of the stress that the fiber could survive for a 1 second proof stress. However, by preventing the environmental reactants from contacting the silica by means of the silicon oxynitride coating, we find that the stress corrosion is substantially affected. A small stress corrosion susceptibility is still present in our silicon oxynitride coated fiber, but as will be seen, the allowable service stress approaches the proof stress level for this fiber. This remaining stress corrosion susceptibility indicates that the amorphous vitreous silicon oxynitride coating experiences stress - assisted crack growth, but at a greatly reduced rate than that found for amorphous SiO_2.

The relationship between stress S_s and mean time to failure t_s under static stress is[32,33]:

$$\log S_s = -u \log t_s + u \log \left[BS_i \left(\frac{1-2u}{u} \right) \right], \qquad (13)$$

where S_i is the inert strength of the weakest flaw, B is a constant for a given glass composition, crack geometry and environment, and u is the

fatigue parameter. The fatigue parameter u is the inverse of the crack velocity exponent n. For fatigue resistant fibers, n becomes large. Experimentally, n is determined through a least squares fit (as discussed below), and when it becomes large it becomes so poorly defined that it can confuse rather than clarify the comparison of fiber properties. For example, $u = 0.005 \pm 0.003$ corresponds to $n = 200$ (+300, -75).

In addition to performing static fatigue lifetime tests, we measure u with stress-rate dependent tensile tests, which are much less time consuming and which have been shown to yield the same fatigue parameter[34]. In these tests, the mean failure stress S_d varies with applied stress rate $\dot{S}$ according to[32,33]

$$\log S_d = \left(\frac{u}{1+u}\right) \log \dot{S} + \left(\frac{u}{1+u}\right) \log \left[\left(\frac{1+u}{u}\right) BS_i \left(\frac{1-2u}{u}\right)\right], \quad (14)$$

where the parameters are the same as in Equation (13). We obtain u from the slope of $\log S_d$ vs. $\log \dot{S}$ and obtain $\left[BS_i \left(\frac{1-2u}{u}\right)\right]$ from the intercept. Using the parameters determined from the strain rate test, we can use Equation (13) to plot a prediction of t_s vs. S_s.

For conventional fibers with a pure SiO_2 surface, u is 0.035 - 0.060 (n= 16 - 29)[34] depending upon humidity, while the fast fracture strength (at $\dot{\varepsilon} = 0.002\ s^{-1}$) is 4.9 GPa. The static fatigue lifetime of such a fiber is shown in Figure 32 (for u = 0.050). Examination of this figure reveals what properties a fatigue-resistant fiber would need in order to outperform the conventional one. For example, a fiber having u = 0 ($n = \infty$) and a fast fracture strength of 2.9 GPa would survive higher static stresses than a conventional fiber in any static test lasting longer than 1 day.

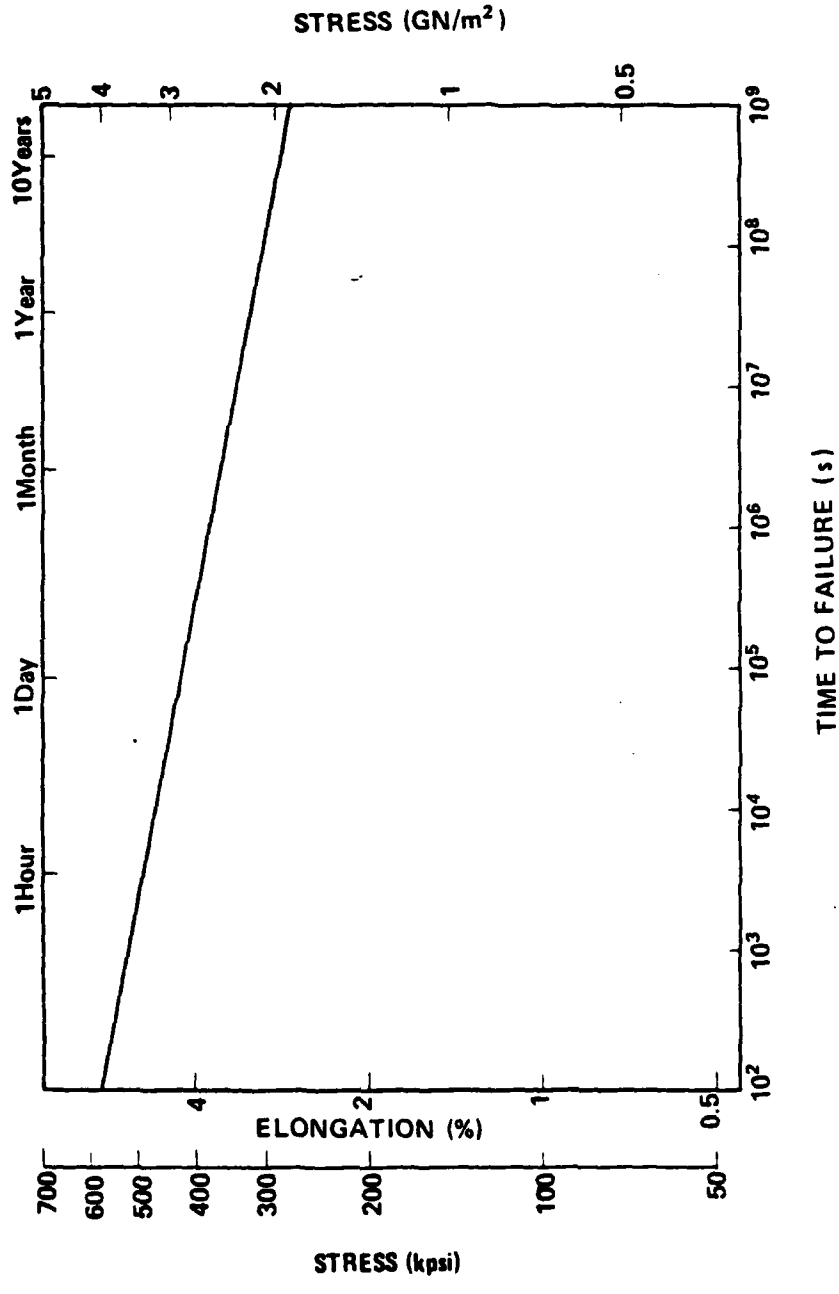

Figure 32. Mean time to failure vs. static applied stress for typical conventional fiber with SiO_2 surface. Fast fracture strength = 4.9 GPa, u = 0.050 (n = 20).

5.2 Dynamic Fatigue Results

Table IV summarizes results of the stress-rate dependence tests (dynamic fatigue) performed with the Instron Tensile Tester as described above. This table includes the 140 μm diameter silicon oxynitride coated fibers (similar results have been obtained in the less extensive tests performed to date on 125 μm diameter silicon oxynitride coated fibers.

The fatigue parameter u (determined from linear regression) is listed, as well as the projected static stress required for 1 hour and 100 year lifetimes based upon Equation 13. When only the carrier gas is present (e.g. #1253) there is no oxynitride coating and the fatigue coefficient is $u = .088 \pm .003$, which is within the range typically found for conventional fused silica fiber. With the normal reaction conditions (partial pressures of .494/.494/.013), the fatigue parameter is always <0.009. When the partial pressures of the reactants are reduced by a factor of three (#1251) the fatigue parameter is higher. When the N_2 flow is off, the fatigue parameter is higher once again. This behavior indicates that there is an optimum range of the ratio of [reactant partial pressure]/[carrier gas partial pressure].

5.3 Static Fatigue Results

Static Fatigue tests of silicon oxynitride coated fibers (and conventional fibers) have been performed using the mandrel technique. Sections of fiber, 1-3 m in length, are helically wound on stainless steel rods of uniform precisely measured diameter. Low winding tension of 30-50g (≈ 20-35 MPa) is used so that the stress in the fiber is determined entirely by its bending curvature. For a fiber of diameter d_f, the strain ε at the surface of the fiber is

$$\varepsilon(\phi) = \frac{d_f}{2R} \cos\phi \quad , \qquad (15)$$

Table IV. Dynamic fatigue of 140 μm diameter silicon oxynitride coated HP fibers.

Fiber No.	Partial Pressure N_2	NH_3	SiH_4	u	Projected static failure stress (GPa) 1 hr	100 yr
1150	0	.978	.022	.0097 ± .0141	1.96 ± .21	1.71 ± .36
1170	.494	.494	.012	.0130 ± .0280	2.36 ± .45	1.98 ± .76
1240	.494	.494	.012	.0122 ± .0101	2.57 ± .20	2.17 ± .41
1251	.830	.166	.004	.0151 ± .0247	1.85 ± .32	1.50 ± .60
1252	.494	.494	.012	.0078 ± .0125	2.30 ± .22	2.06 ± .45
1253	1.00	0	0	.1178 ± .0293	1.73 ± .30	0.35 ± .15
1290	.494	.494	.012	.0093 ± .0094	2.25 ± .16	1.98 ± .33
1300	0	.977	.023	.0149 ± .0134	2.11 ± .21	1.72 ± .40
1310	0	.977	.023	.0288 ± .0114	1.73 ± .12	1.17 ± .23
1320	0	.987	.012	.0344 ± .0274	2.37 ± .41	1.48 ± .65
1570	.494	.494	.012	.0070 ± .0124	2.40 ± .21	2.18 ± .44

where R is the radius of curvature of the fiber and ϕ is the azimuthal angle relative to the plane of the bend. The outer surface of the fiber (ϕ=0°) is under tensile stress while the inner surface of the fiber (ϕ = 180°) is under compressive stress.

The fracture of a fiber under bending stress will normally occur at cracks on the outer surface of the fiber because the stress is highest there. In actuality, a sizeable fraction of the fiber surface area experiences nearly the maximum tensile stress (14% of the surface area experiences stress $\geq$ 90% of the maximum stress). So the effective gauge length of fiber under test is approximately 14% of the 1-3 m total length which is wound around the mandrel.

To set up our mandrel tests, we hold the mandrel in a special fixture having one chuck to hold each end. A motor rotates the assembly at constant speed while a level winder guides the fiber onto the mandrel. A small braking tension is applied to the payout axle to keep the fiber snugly wrapped around the mandrel, and the ends are secured by wrapping tape around them.

The time-to-failure of the fibers is monitored by visually checking the mandrels daily. The fibers under test are only coated with silicone, and will unwind from the mandrel when they fail. Typical life-test data is shown in Figure 33, where it is compared to the predictions from the dynamic fatigue test. We have excellent agreement between the predictions and the measurements. The scatter in the static fatigue data for conventional fibers probably originates from variations in the environment or the chemical conditions at the surface of the fiber.

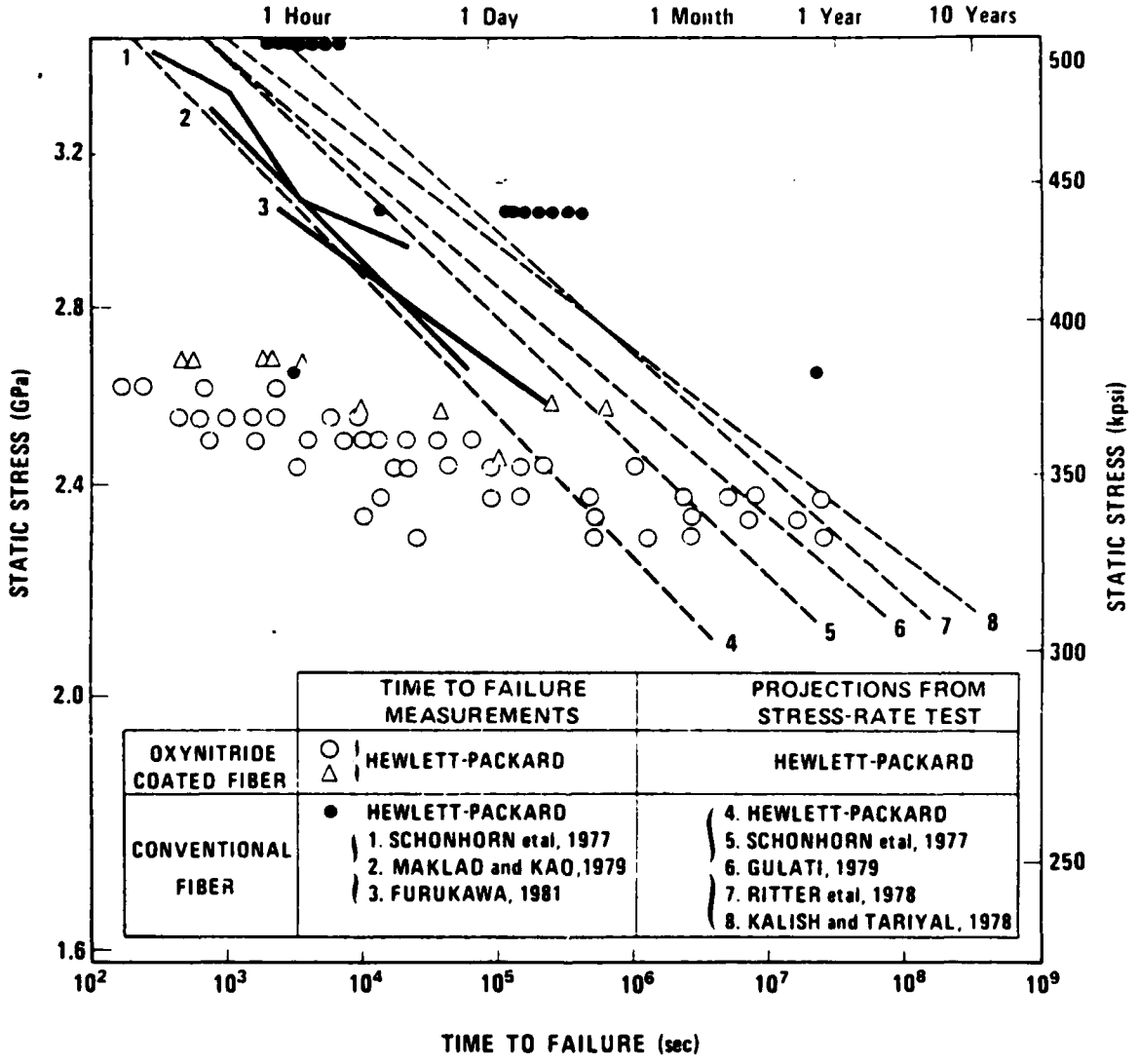

Figure 33. Static fatigue comparison between oxynitride coated fiber and conventional fiber at 22°C in air at 50% R.H.

According to these data, the silicon oxynitride coated fiber has a longer mean time to failure than the conventional fiber at any stress lower than 2.3 ± 0.1 GPa (330 ± 10 kpsi). For the oxynitride coated fiber, the static fatigue strength for 30 year stress duration is 85% of that for 1 second stress duration. In contrast, the static fatigue strength of conventional fiber for 30 year stress duration is 37% of that for 1 second stress duration. The substantially reduced static fatigue of the silicon oxynitride coated fiber has a dramatic impact on the proof stress requirement to assure a specific lifetime under a specific static stress. For example, to assure a lifetime of 30 years under 2.0 GPa static stress, the silicon oxynitride coated fiber would need to pass a 1 second proof stress at 2.35 GPa, while a conventional fiber would need to pass a 1 second proof stress at 5.40 GPa.

Static fatigue tests using mandrels are also conducted in deionized water at temperatures of ambient to +85°C. Figure 34 shows fatigue data for both oxynitride coated and uncoated fibers. In both cases the lifetime is degraded compared to ambient conditions. However, the oxynitride coated fiber still has substantially less time dependence of strength compared to the conventional fiber.

Additional mandrel tests have been conducted in a Blue M(TM) environmental chamber at temperatures up to 85°C and humidities up to 85% R.H. Figure 35 shows data from these tests, which are quite similar to those in water immersion.

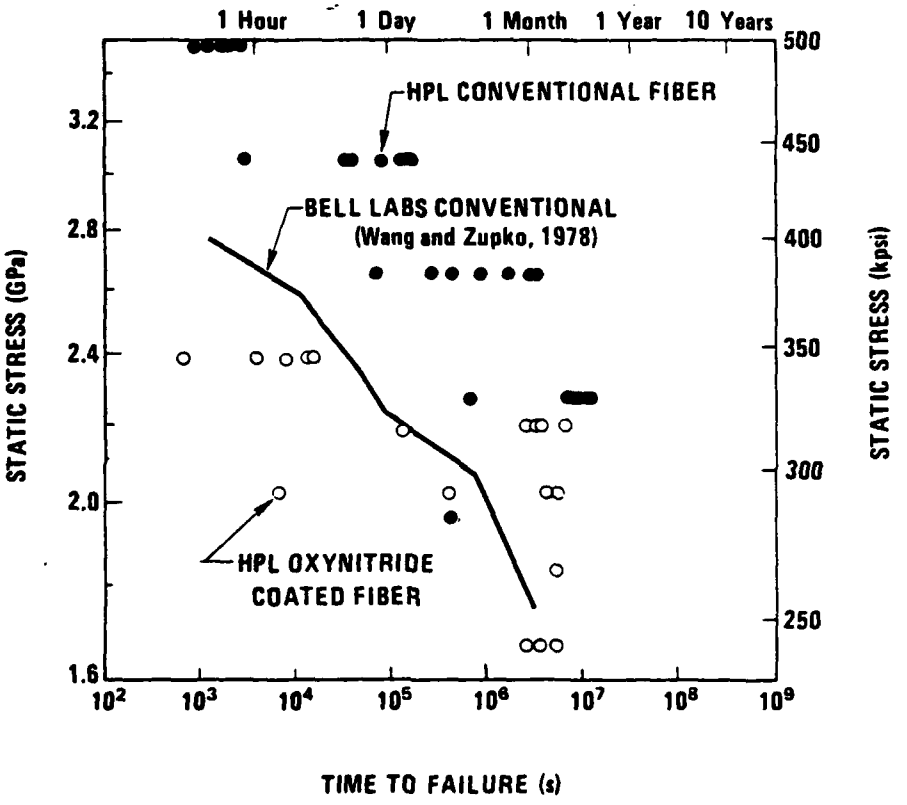

Figure 34. Static fatigue at 22°C for fibers immersed in deionized water, compared to Bell Labs data at 33°C and 90% R.H.

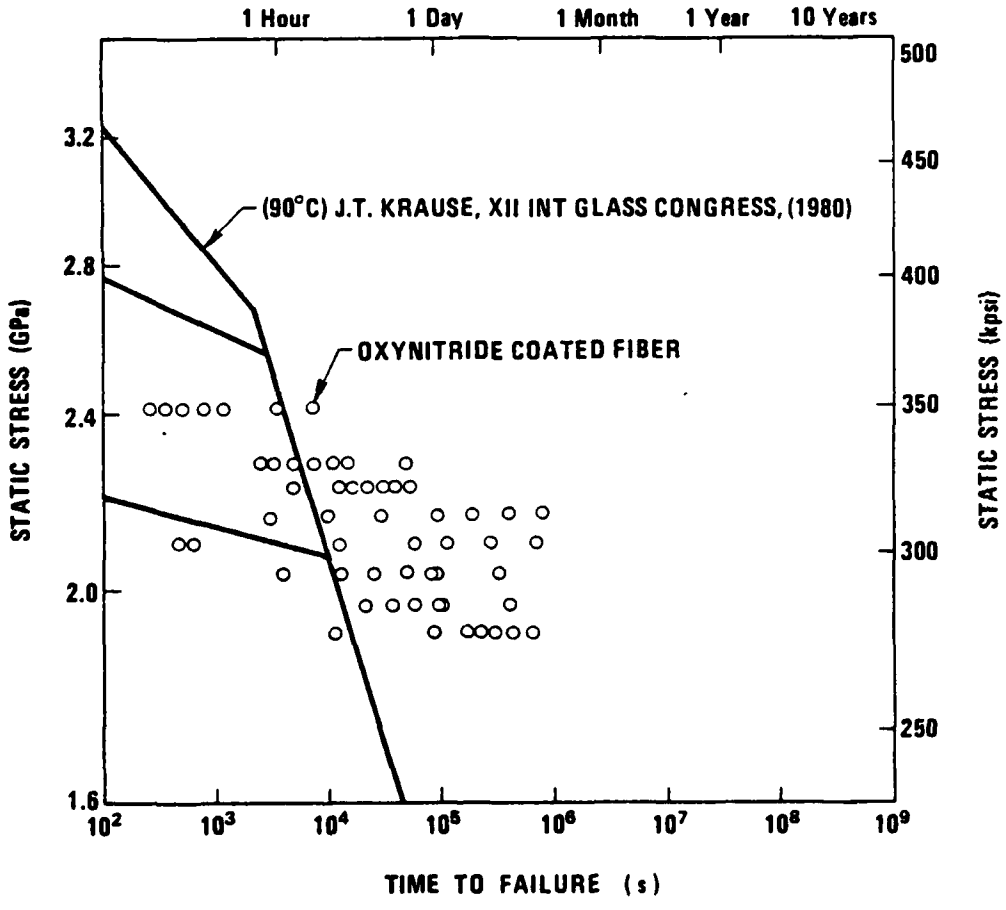

Figure 35. Static fatigue data in 80°C water.

5.4 Cyclic Fatigue

Polycrystalline coatings have been used by other workers[4] to achieve fatigue resistance in silica optical fibers. However, such coatings are susceptible to a serious cyclic fatigue problem arising from the anisotropic nature of each crystallite and the relatively low yield strain. Under cyclic strain of only 0.7%, polycrystalline aluminum films experience substantial deformation, which leads to optical loss in the fiber from microbending, and also to the likely development of pinholes. These pinholes allow atmospheric water to directly attack the silica surface, nullifying the fatigue resistance of the coating.

The silicon oxynitride films being fabricated in this contract are vitreous and amorphous. Because of their isotropic nature, they should not form pinholes under cyclic strain. Also, the coating thickness is a thousand times less than the metallic coatings discussed above[4], greatly reducing the potential for microbending loss. The yield strain is not known for thin amorphous silicon oxynitride films of the type we are fabricating, and it is possible that some sort of deformation might occur at high strains if the film yields. To check the behavior under cyclic strain, we used a section of fiber 1291 (gauge length 0.35 m) on our Instron tensile tester, and cycled the load between 0 and 34 N (corresponding to 0% and 3.1% strain, respectively) at a rate of 1 cycle per 27.5 s. For this fiber, the fast fracture strength was 2.5 GPa. The fiber was cycled > 6,000 times without fracturing, and the test was terminated only so the Instron could be used for other purposes. This result indicates that no catastrophic changes in the silicon oxynitride film were caused by cyclic loading.

6.0 Optical Properties

The attenuation of the HP silicon oxynitride coated fibers is unaffected by the oxynitride coating. One test demonstrating this involved the pulling of one preform in two sections: one with the silicon oxynitride coating and the other without. The attenuation measurement of the oxynitride coated portion (see Figure 36) was 4.85 dB/km at 820 nm. There was no discernable difference in attenuation between the oxynitride coated and non-oxynitride coated portions of fiber.

To further test for any possible attenuation in the fiber, we have conducted another cyclic loading test, cycling ten times between 0% and 3.0% strain using a 432 m section of fiber 1431. The stress was applied as the fiber passed between two capstans during a rewinding operation, and the stress duration at each point along the fiber length was 1.0 second. The attenuation of the fiber at 820 nm was measured before and after the ten cycles. The two attenuations were equal within the ± 0.2 dB accuracy of our attenuation measurement system, showing that no measurable microbending attenuation had been caused by cyclic loading.

Preliminary optical absorption measurements on short pieces of oxynitride coated fiber indicate increased absorption of cladding modes at 400 - 700 nm caused by the silicon oxynitride layer. This absorption has no effect upon core modes as evidenced by the attenuation measurements, but the measurement appears to be a useful tool for monitoring the thickness and stoichiometry of the film.

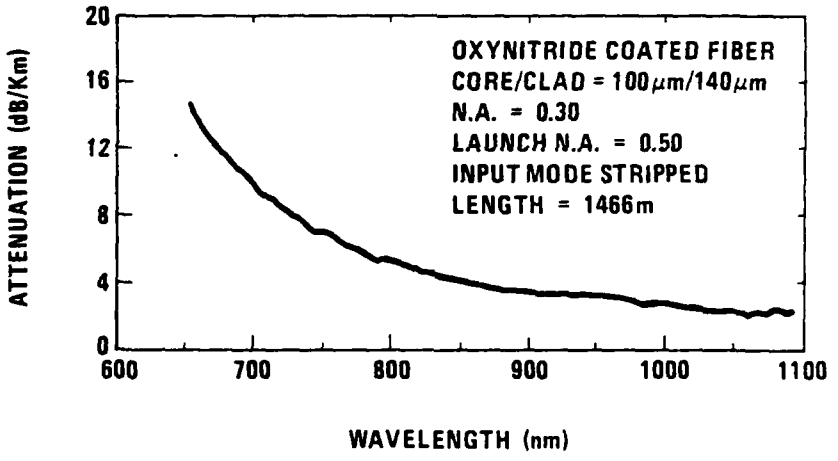

Figure 36. Spectral attenuation of silicon oxynitride coated fiber.

7.0 CONCLUSIONS

A reproducible silicon oxynitride coating process has been demonstrated which produces fiber having less than one-sixth the static fatigue susceptibility (as measured by the fatigue parameter u) of conventional fiber. It does have a fast fracture strength only 60% of that of conventional fiber, but even so, its extrapolated static fatigue lifetime is longer than that of conventional fiber for all static applied stresses lower than 2.2 GPa. The reduced fast fracture strength is caused by either tensile stresses in the film or by reduced film strength compared to that of the pristine silica fiber. The silicon oxynitride coating does not cause any measurable increase in fiber attenuation, even after cyclic stressing 10 times to 3.0% strain. No cyclic fatigue is evident after > 6,000 cycles at 3.0% strain. The silicon oxynitride coated fiber has the same incidence of flaws in the 0 - 2.1 GPa range as conventional fiber pulled in our lab, indicating that the silicon oxynitride coating does not introduce additional flaws. Lengths up to 1350 m have successfully passed the 2.1 GPa test with high yield as shown in Table II on page 44. A length of silicon oxynitride coated fiber passing such a 2.1 GPa test is assured of surviving for 30 years at 1.8 GPa, while a conventional fiber passing the same test is only assured of surviving 30 years at 0.8 GPa.

8.0 REFERENCES

1. "Introduction to Ceramics", W. D. Kingery, H. K. Bowen and D. R. Uhlmann, Wiley, New York, 1976.

2. M. S. Maklad, S. M. Oh and P. L. Narasimham, Digest of Extended Abstracts, Conference on Physics of Fiber Optics, American Ceramic Society 82nd Annual Meeting, April 27-30, 1980, Chicago, Illinois, p. 24.

3. T. T. Wang and H. M. Zupko, J. Mater. Sci. 13, p. 2241 (1978).

4. J. A. Wysocki, G. R. Blair and B. D. Robertson, Digest of Extended Abstracts, Conference on Physics of Fiber optics, American Ceramic Society 82nd Annual Meeting, April 27-30, 1980, Chicago, Illinois, p. 32.

5. M. L. Stein and S. Aisenberg, Digest of Extended Abstract, Conference on Physics of Fiber Optics, American Ceramic Society 82nd Annual Meeting, April 27-80, 1980, Chicago, Illinois, p. 29.

6. S. Lin, J. Electrochemical Society 124, No. 12, p. 1945, (1977).

7. D. Dong, E. A. Irene and D. R. Young, J. Electrochemical Society 125, No. 5, p. 819 (1978).

8. H. H. Madden, J. Electrochemical Society 128, No. 3, p. 625 (1981).

9. A. C. Airey, S. Clarke and P. Popper, Proceedings British Ceramic Society 22, p. 305 (1973).

10. R. Gereth and W. Scherber, J. Electrochemical Society 119, No. 9, p. 1248 (1972).

11. T. C. Hall, R. L. Long and J. W. Peters, Final Technical Report, Contract # AFML-TR-77-74, 1977.

12. "Handbook of Electronic Materials" Vol. 3, J. T. Milek, IFI/Plenum, New York, 1971.

13. E. N. Sickafus, Phys. Rev. B 16, pp. 1436 and 1448 (1977).

14. N. R. Draper and H. Smith, "Applied Regression Analysis", Wiley, New York (1966).

15. R. Hiskes, Digest of Extended Abstracts, Topical Meeting on Optical Fiber Communication, Washington, D.C., March, 1979.

16. C. J. Phillips, American Scientist 53, p. 20 (1965).

17. A. A. Griffith, Phil. Trans. Roy. Soc. A221, p. 163 (1920).

18. W. B. Hillig. J. Applied Physics 32, p. 741 (1961).

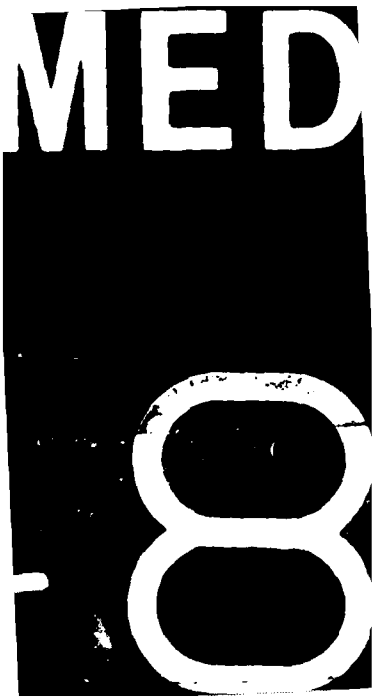
MED
8